

LSST: FROM SCIENCE DRIVERS TO REFERENCE DESIGN AND ANTICIPATED DATA PRODUCTS

Ž. IVEZIĆ¹, J.A. TYSON², R. ALLSMAN³, J. ANDREW⁴, R. ANGEL⁵, T. AXELROD³, J.D. BARR⁴, A.C. BECKER¹, J. BECLA⁶, C. BELDICA⁷, R.D. BLANDFORD⁶, W.N. BRANDT⁸, J.S. BULLOCK⁹, D.L. BURKE⁶, S. CHANDRASEKHARAN⁴, S. CHESLEY¹⁰, C.F. CLAVER⁴, A. CONNOLLY¹, K.H. COOK¹¹, A. COORAY⁹, C. CRIBBS⁷, R. CUTRI¹², G. DAUES⁷, F. DELGADO¹³, H. FERGUSON¹⁴, J.C. GEARY¹⁵, P. GEE², D.K. GILMORE⁶, W.J. GRESSLER⁴, C. HOGAN¹, M.E. HUFFER⁶, S.H. JACOBY³, B. JAIN¹⁶, J.G. JERNIGAN¹⁷, R.L. JONES¹, M. JURIC¹⁸, S.M. KAHN⁶, J.S. KALIRAI¹⁹, J.P. KANTOR³, D. KIRKBY⁹, L. KNOX², V.L. KRABBENDAM⁴, S. KRUGHOFF¹, S. KULKARNI²⁰, R. LAMBERT¹³, D. LEVINE¹², M. LIANG⁴, K-T. LIM⁶, R.H. LUPTON²¹, P. MARSHALL²², S. MARSHALL⁶, M. MAY²⁴, M. MILLER⁴, D.J. MILLS⁴, D.G. MONET²³, D.R. NEILL⁴, M. NORDBY⁶, P. O'CONNOR²⁴, J. OLIVER²⁵, S.S. OLIVIER¹¹, R.E. OWEN¹, J.R. PETERSON²⁶, C.E. PETRY⁵, F. PIERFEDERICI³, S. PIETROWICZ⁷, R. PIKE²⁷, P.A. PINTO⁵, R. PLANTE⁷, V. RADEKA²⁴, A. RASMUSSEN⁶, W. ROSING²⁸, A. SAHA⁴, T.L. SCHALK²⁹, R.H. SCHINDLER⁶, D.P. SCHNEIDER⁸, G. SCHUMACHER¹³, J. SEBAG⁴, L.G. SEPPALA¹¹, I. SHIPSEY²⁵, N. SILVESTRI¹, J.A. SMITH³⁰, R.C. SMITH¹³, M.A. STRAUSS²¹, C.W. STUBBS²⁵, D. SWEENEY³, A. SZALAY³¹, J.J. THALER³², D. VANDEN BERK⁸, M. WARNER¹³, B. WILLMAN²⁵, D. WITTMAN², S.C. WOLFF⁴, W.M. WOOD-VASEY²⁵, AND H. ZHAN², FOR THE LSST COLLABORATION

A living LSST document; version 1.0 of May 15, 2008

ABSTRACT

In the history of astronomy, major advances in our understanding of the Universe frequently arise from dramatic improvements in our ability to accurately measure astronomical quantities. Aided by rapid progress in information technology, current sky surveys are changing the way we view and study the Universe. Next-generation surveys will maintain this revolutionary progress. We focus here on the most ambitious survey currently planned in the visible band, the Large Synoptic Survey Telescope (LSST). LSST will have unique survey capability in the faint time domain. The LSST design is driven by four main science themes: probing dark energy and dark matter, taking an inventory of the Solar System, exploring the transient optical sky, and mapping the Milky Way. LSST will be a large, wide-field ground-based system designed to obtain multiple images covering the sky that is visible from Cerro Pachón in Northern Chile. The current baseline design, with an 8.4m (6.5m effective) primary mirror, a 9.6 deg² field of view, and a 3.2 Gigapixel camera, will allow about 10,000 square degrees of sky to be covered using pairs of 15-second exposures in two photometric bands every three nights on average, with typical 5 σ depth for point sources of $r \sim 24.5$. The system is designed to yield high image quality as well as superb astrometric and photometric accuracy. The survey area will include 30,000 deg² with $\delta < +34.5^\circ$, and will be imaged multiple times in six bands, *ugrizy*, covering the wavelength range 320–1050 nm. The project is scheduled to have first light in 2014 and the beginning of survey operations in 2015. About 90% of the observing time will be devoted to a deep-wide-fast survey mode which will observe a 20,000 deg² region about 1000 times (summed over all six bands) during the anticipated 10 years of operations, and yield a coadded map to $r \sim 27.5$. These data will result in databases including 10 billion galaxies and a similar number of stars, and will serve the majority of science programs. The remaining 10% of the observing time will be allocated to special programs such as a Very Deep and Fast time domain survey. We illustrate how the LSST science drivers led to these choices of system parameters, and describe the expected data products and their characteristics. The LSST data products will be available to the public and scientists around the world – everyone will be able to view and study a high-definition color movie of the deep Universe.

Subject headings: astronomical data bases: atlases, catalogs, surveys — Solar System — stars — the Galaxy — galaxies — cosmology

¹ University of Washington, Dept. of Astronomy, Box 351580, Seattle, WA 98195

² Physics Department, University of California, One Shields Avenue, Davis, CA 95616

³ LSST Corporation, 933 N. Cherry Avenue, Tucson, AZ 85721

⁴ National Optical Astronomy Observatory, 950 N. Cherry Ave, Tucson, AZ 85719

⁵ Steward Observatory, The University of Arizona, 933 N Cherry Ave., Tucson, AZ 85721

⁶ Kavli Institute for Particle Astrophysics and Cosmology, Stanford Linear Accelerator Center, Stanford University, Stanford, CA 94025

⁷ NCSA, University of Illinois at Urbana-Champaign, 1205 W. Clark St., Urbana, IL 61801

⁸ Department of Astronomy and Astrophysics, The Pennsylvania State University, 525 Davey Lab, University Park, PA 16802

⁹ Center for Cosmology, University of California, Irvine, CA 92697

¹⁰ Jet Propulsion Laboratory, California Institute of Technology, Pasadena, CA 91109

¹¹ Lawrence Livermore National Laboratory, 7000 East Avenue, Livermore, CA 94550

¹² IPAC, California Institute of Technology, MS 100-22, Pasadena, CA 91125

¹³ Cerro Tololo InterAmerican Observatory, La Serena, Chile

¹⁴ Space Telescope Science Institute, 3700 San Martin Drive, Baltimore, MD 21218

¹⁵ Smithsonian Astrophysical Observatory, 60 Garden St., Cambridge MA 02138

¹⁶ Department of Physics & Astronomy, University of Pennsylvania, 209 South 33rd Street, Philadelphia, PA 19104-6396

¹⁷ Space Sciences Lab, University of California, 7 Gauss Way,

1. INTRODUCTION

Major advances in our understanding of the Universe have historically arisen from dramatic improvements in our ability to "see". We have developed progressively larger telescopes over the past century, allowing us to peer further into space, and further back in time. With the development of advanced instrumentation – imaging, spectroscopic, and polarimetric – we have been able to parse radiation detected from distant sources over the full electromagnetic spectrum in increasingly subtle ways. These data have provided the detailed information needed to construct physical models of planets, stars, galaxies, quasars, and larger structures.

Until recently, most astronomical investigations have focused on small samples of cosmic sources or individual objects. This is because our largest telescope facilities typically had rather small fields of view, and those with large fields of view could not detect very faint sources. With all of our existing telescope facilities, we have still surveyed only a minute volume of the observable Universe.

Over the past two decades, however, advances in technology have made it possible to move beyond the traditional observational paradigm and to undertake large-scale sky surveys. As vividly demonstrated by surveys such as the Sloan Digital Sky Survey (SDSS; York et al. 2000), the Two Micron All Sky Survey (2MASS; Skrutskie et al. 2006), and the Galaxy Evolution Explorer (GALEX; Martin et al. 2006), to name but a few, sensitive and accurate multi-color surveys over a large fraction of the sky enable an extremely broad range of new scientific investigations. These projects, based on a synergy of advances in telescope construction, detectors, and above all, information technology, have dramatically impacted nearly all fields of astronomy – and many areas of fundamental physics. In addition, the recent world-wide attention received by Google Sky³³ (Scranton et al. 2007)

demonstrates that the impact of sky surveys extends far beyond fundamental science progress and reaches all of society.

Motivated by the evident scientific progress enabled by large sky surveys, three nationally-endorsed reports by the U.S. National Academy of Sciences³⁴ concluded that a dedicated ground-based wide-field imaging telescope with an effective aperture of 6–8 meters is a high priority for planetary science, astronomy, and physics over the next decade. The Large Synoptic Survey Telescope (LSST) described here is such a system. The LSST will be a large, wide-field ground-based telescope designed to obtain multi-band images over a substantial fraction of the sky every few nights. The survey will yield contiguous overlapping imaging of over half the sky in six optical bands, with each sky location visited about 1000 times over 10 years.

The purpose of this paper is to provide an overall summary of the main LSST science drivers and how they led to the current system design parameters (§ 2), to describe anticipated data products (§ 3), and to provide a few examples of the science programs that LSST will enable (§ 4). The community involvement is discussed in § 5, and broad educational and societal impacts in § 6. The concluding remarks are presented in § 7. This publication will be maintained at the arxiv.org site³⁵, and will also be available from the LSST website (www.lsst.org). The latest version should be consulted for the most up-to-date information about the LSST system.

2. FROM SCIENCE DRIVERS TO REFERENCE DESIGN

The most important characteristic that determines the speed at which a system can survey a given sky area to a given depth (faint flux limit) is its *étendue* (or *grasp*), the product of its primary mirror area and the field-of-view area (assuming that observing conditions such as seeing, sky brightness, etc., are fixed). The effective *étendue* for LSST will be greater than 300 m² deg², which is more than an order of magnitude larger than that of any existing facility. For example, the SDSS, with its 2.5-m telescope (Gunn et al. 2006) and a camera with 30 imaging CCDs (Gunn et al. 1998), has an effective *étendue* of only 5.9 m² deg².

The range of scientific investigations which will be enabled by such a dramatic improvement in survey capability is extremely broad. Guided by the community-wide input assembled in the report of the Science Working Group of the LSST³⁶, the LSST is designed to achieve goals set by four main science themes:

1. Probing Dark Energy and Dark Matter
2. Taking an Inventory of the Solar System
3. Exploring the Transient Optical Sky
4. Mapping the Milky Way

³⁴ Astronomy and Astrophysics in the New Millennium, NAS 2001; Connecting Quarks with the Cosmos: Eleven Science Questions for the New Century, NAS 2003; New Frontiers in the Solar System: An Integrated Exploration Strategy, NAS 2003.

³⁵ <http://lanl.arxiv.org/abs/0805.2366>

³⁶ Available as <http://www.lsst.org/Science/docs/DRM2.pdf>

Berkeley, CA 94720-7450

¹⁸ Institute for Advanced Study, 1 Einstein Drive, Princeton, NJ 08540

¹⁹ Lick Observatory, University of California, Santa Cruz, CA 95060

²⁰ Astronomy Department, California Institute of Technology, 1200 East California Blvd., Pasadena CA 91125

²¹ Department of Astrophysical Sciences, Princeton University, Princeton, NJ 08544

²² Physics Department, University of California, Santa Barbara, CA 93106

²³ U.S. Naval Observatory Flagstaff Station, 10391 Naval Observatory Road, Flagstaff, AZ 86001

²⁴ Brookhaven National Laboratory, Upton, NY 11973

²⁵ Departments of Physics and Astronomy, Center for Astrophysics, Harvard University, 60 Garden St., Cambridge, MA 02138

²⁶ Department of Physics, Purdue University, 525 Northwestern Ave., West Lafayette, IN 47907

²⁷ Google Inc., 1600 Amphitheatre Parkway Mountain View, CA 94043

²⁸ Las Cumbres Observatory, 6740 Cortona Dr. Suite 102, Santa Barbara, CA 93117

²⁹ Institute of Particle Physics, University of California–Santa Cruz, 1156 High St., Santa Cruz, CA 95060

³⁰ Austin Peay State University, Clarksville, TN 37044

³¹ Department of Physics and Astronomy, The John Hopkins University, 3701 San Martin Drive, Baltimore, MD 21218

³² University of Illinois, Physics and Astronomy Departments, 1110 W. Green St., Urbana, IL 61801

³³ <http://earth.google.com/sky/>

Each of these four themes itself encompasses a variety of analyses, with varying sensitivity to instrumental and system parameters. These themes fully exercise the technical capabilities of the system, such as photometric and astrometric accuracy and image quality. About 90% of the observing time will be devoted to a deep-wide-fast (main) survey mode. The working paradigm is that all scientific investigations will utilize a common database constructed from an optimized observing program (the main survey mode), such as that discussed in Section 3. Here we briefly describe the science goals and the most challenging requirements for the telescope and instrument that are derived from those goals, which will inform the overall system design decisions discussed below. For a more detailed discussion, we refer the reader to the LSST Science Requirements Document³⁷, as well as to the numerous LSST poster presentations at the recent meetings of the AAS³⁸.

2.1. The Main Science Drivers

The main science drivers are used to optimize various system parameters. Ultimately, in this high-dimensional parameter space, there is a manifold defined by the total project cost. The science drivers must both justify this cost, as well as provide guidance on how to optimize various parameters while staying on the cost manifold.

Here we summarize the dozen most important interlocking constraints on data properties placed by the four main science themes:

1. The depth of a single visit (an observation consisting of two back-to-back exposures of the same region of sky)
2. Image quality
3. Photometric Accuracy
4. Astrometric Accuracy
5. Optimal exposure time
6. The filter complement
7. The distribution of revisit times (i.e., the cadence of observations), including the survey lifetime
8. The total number of visits to a given area of sky
9. The coadded survey depth
10. The distribution of visits on the sky, and the total sky coverage
11. The distribution of visits per filter
12. Data processing and data access (e.g., time delay for reporting transient sources and the software contribution to measurement errors)

We present a detailed discussion of how these science-driven data properties are transformed to system parameters below.

2.1.1. Probing Dark Energy and Dark Matter

Current models of cosmology require the existence of both dark matter and dark energy to match observational constraints (Spergel et al. 2007; Riess et al. 2007; Tegmark et al. 2006; and references therein). Dark energy affects the cosmic history of both the Hubble expansion and mass clustering. If combined, different types of probes of the expansion history and structure history can lead to tight constraints (a percent level precision) on the dark energy equation of state and other cosmological parameters. These tight constraints arise because each technique depends on the cosmological parameters or errors in different ways. The most powerful probes include weak gravitational lens cosmic shear (WL), baryon acoustic oscillations (BAO), supernovae (SN), and cluster counting – all as functions of redshift. Using the cosmic microwave background as normalization, the combination of these probes can yield the needed precision to distinguish among models of dark energy (Zhan 2006, and references therein). In addition, time-resolved strong galaxy and cluster lensing probes the physics of dark matter. This is because the positions and profiles of multiple images of a source galaxy depend sensitively on the total mass distribution, including the dark matter, in the lensing object.

Three major programs from this science theme provide unique and independent constraints on the system design:

- Weak lensing of galaxies,
- Baryon Acoustic Oscillations
- Type Ia Supernovae.

Weak lensing (WL) techniques can be used to map the distribution of mass as a function of redshift and thereby trace the history of both the expansion of the Universe and the growth of structure (e.g., Hu & Tegmark 1999; Wittman et al. 2000; for a review see Bartelmann & Schneider 2001). Weak lensing of galaxies as a function of redshift probes both the evolution of structure over cosmic time and determines dimensionless ratios of distances versus cosmic time, giving multiple independent constraints on the nature of dark energy. These investigations require deep wide-area multi-color imaging with stringent requirements on shear systematics in at least two bands, and excellent photometry in all bands (a requirement shared with BAO.) The strongest constraints on the LSST image quality come from this science program. In order to control systematic errors in shear measurement, it is mandatory to obtain the desired depth with many short exposures (which enables reconstruction of galaxy shapes with minimum systematic error). Detailed simulations of weak lensing techniques show that, in order to obtain a sample of ~ 3 billion lensing galaxies, the coadded map must cover $\sim 20,000$ deg², and reach a depth of $r \sim 27.5$ (5σ for point sources), with several hundred exposures per field and sufficient signal-to-noise in at least five other bands to obtain accurate photometric redshifts. This depth optimizes the number of measured galaxies in ground-based seeing, and allows their detection in significant numbers to beyond a redshift of two. It is anticipated that optimal science analysis of

³⁷ Available at <http://www.lsst.org/Science/docs.shtml>

³⁸ See <http://www.lsst.org/Meetings/AAS/2008/AAS211.shtml>

weak lensing will place strong constraints on data processing software, such as simultaneous analysis of all the available images rather than analyzing a deep coadded image (Tyson et al. 2008).

Type Ia supernovae (SN) provided the first evidence that the expansion of the Universe is accelerating (Riess et al. 1998; Perlmutter et al. 1999). To fully exploit the supernovae science potential, light curves sampled in multiple bands every few days over the course of a few months are required. This is essential to search for systematic differences in supernova populations (e.g., due to progenitor channels) which may masquerade as cosmological effects, as well as to determine photometric redshifts from the supernovae themselves. Unlike other cosmological probes, even a single object can provide useful constraints and, therefore, a large number of SN across the sky can enable a high angular resolution search for any dependence of dark energy properties on direction, which would be an indicator of new physics. Given the expected SN flux distribution, the single visit depth should be at least $r \sim 24$. Good image quality is required to separate SN photometrically from their host galaxies. Observations in at least five photometric bands are necessary to ensure that, for any given supernova, light curves in several bands will be obtained (due to the spread in redshift). The importance of K-corrections to supernova cosmology implies that the calibration of the relative offsets in photometric zero points between filters and the knowledge of the system response functions, especially near the edges of bandpasses, must be accurate to about 1% (Wood-Vasey et al. 2007). Similar photometric accuracy is required for photometric redshifts of galaxies. Deeper data ($r > 26$) for small areas of the sky can extend the discovery of SN to a mean redshift of 0.7 (from ~ 0.5 for the main survey), with some objects beyond $z \sim 1$ (Garnavich et al. 2005; Pinto et al. 2005). The added statistical leverage on the “pre-acceleration” era would improve constraints on the properties of dark energy as a function of redshift.

2.1.2. *Taking an Inventory of the Solar System*

The small-body populations in the Solar System, such as asteroids, trans-Neptunian objects (TNOs) and comets, are remnants of its early assembly. The history of accretion, collisional grinding, and perturbation by existing and vanished giant planets is preserved in the orbital elements and size distributions of those objects. Collisions in the main asteroid belt between Mars and Jupiter still occur, and occasionally objects are ejected on orbits that may take them on a collision course with Earth.

As a result, the Earth orbits within a swarm of asteroids; some number of these objects will ultimately strike the Earth’s surface. In December 2005, the U.S. Congress directed³⁹ NASA to implement a near-Earth object (NEO) survey that would catalog 90% of NEOs larger than 140 meters by 2020. About 20% of NEOs, the potentially hazardous asteroids or PHAs, are in orbits that pass sufficiently close to Earth’s orbit, to within 0.05 AU, that perturbations with time scales of a century can lead to intersections and the possibility of collision. In order to fulfill the Congressional mandate us-

ing a ground-based facility, a 10-meter class telescope equipped with a multi-gigapixel camera, and a sophisticated and robust data processing system are required (Ivezić et al. 2007a). The search for NEOs also places strong constraints on the cadence of observations, requiring closely spaced pairs of observations (two or preferably three times per lunation) in order to link observations unambiguously and derive orbits. Individual exposures should be shorter than about 30 seconds each to minimize the effects of trailing for the majority of moving objects. The images must be well sampled to enable accurate astrometry, with absolute accuracy of at least 0.1 arcsec. The images should reach a depth of at least ~ 24.5 (5σ for point sources) in the r band in order to probe the ~ 0.1 km size range at main-belt distances, and to fulfill the Congressional NEO mandate. The photometry should be better than 1-2% to enable color-based taxonomy.

2.1.3. *Exploring the Transient Optical Sky*

Recent surveys have shown the power of measuring variability for studying gravitational lensing, searching for supernovae, determining the physical properties of gamma-ray burst sources, probing the structure of active galactic nuclei, and many other subjects at the forefront of astrophysics (Tyson 2006, and references therein). A wide-area dense temporal coverage to deep limiting magnitudes would enable the discovery and analysis of rare and exotic objects such as neutron star and black hole binaries, novae and stellar flares, gamma-ray bursts and X-ray flashes, active galactic nuclei (AGNs), stellar disruptions by black holes, and possibly new classes of transients, such as binary mergers of black holes (Shields & Bonning 2008). Such a survey likely would detect numerous microlensing events in the Local Group and perhaps beyond, and open the possibility of discovering planets (e.g., Beaulieu et al. 2006), as well as obtaining spectra of lensed stars in distant galaxies.

Time-domain science requires large area coverage to enhance the probability of detecting rare events; good time sampling, because light curves are necessary to distinguish certain types of variables and in some cases to infer their properties (e.g., determining the intrinsic luminosity of Type Ia supernovae depends on measurements of their rate of decline); accurate color information to assist with the classification of variable objects; good image quality to enable differencing of images, especially in crowded fields; and rapid data reduction, classification and reporting to the community in order to flag interesting objects for spectroscopic and other investigations with separate facilities. Time scales ranging from 1 min, to constrain the properties of fast faint transients (such as optical flashes associated with gamma-ray bursts; Bloom et al. 2008) and transients recently discovered by the Deep Lens Survey (Becker et al. 2004), to 10 years to study long-period variables and quasars (Kaspi et al. 2007) should be probed over a significant fraction of the sky. It should be possible to measure colors of fast transients, and to reach faint magnitude limits in individual visits (at least the Deep Lens Survey limit of $r \sim 24.5$).

³⁹ For details see <http://neo.jpl.nasa.gov/neo/report2007.html>

2.1.4. Mapping the Milky Way

A major objective of modern astrophysics is to understand when and how galaxies formed and evolved. Arguably the biggest challenge to extragalactic cosmology today concerns the formation of structure on sub-galactic scales, where baryon physics becomes important, and where the nature of dark matter may manifest itself in observable ways. The Milky Way and its environment provide a unique data set for understanding the detailed processes that shape galaxy formation and for testing the small-scale predictions of our standard cosmology. However, we still lack robust answers to two basic questions about our Galaxy:

- What is the detailed structure and accretion history of the Milky Way?
- What are the fundamental properties of all the stars within 300 pc of the Sun?

Key requirements for mapping the Galaxy are large area coverage, excellent image quality to maximize the photometric and astrometric accuracy, especially in crowded fields; photometric precision of at least 1% to separate main sequence and giant stars (e.g., Helmi et al., 2003); and astrometric precision of about 10 mas per observation to enable parallax and proper motion measurements. In order to probe the halo out to its presumed edge at ~ 100 kpc (Ivezić et al. 2003) using numerous main-sequence stars, the total coadded depth must reach $r > 27$, with a similar depth in the g band. To study the metallicity distribution of stars in the Sgr tidal stream (e.g., see Majewski et al. 2003) and other halo substructures at distances beyond the presumed boundary between inner and outer halo (~ 30 kpc, Carollo et al. 2007), the coadded depth in the u band must reach ~ 24.5 . To detect RR Lyrae stars beyond the Galaxy's tidal radius at ~ 300 kpc, the single-visit depth must be $r \sim 24.5$. In order to measure the tangential velocity of stars at a distance of 10 kpc, where the halo dominates over the disk, to within 10 km/s needed to be competitive with large-scale radial velocity surveys, the required proper motion accuracy is at least 0.2 mas/yr. The same accuracy follows from the requirement to obtain the same proper motion accuracy as Gaia (Perryman et al. 2001) at its faint limit ($r \sim 20$). In order to produce a complete sample of solar neighborhood stars out to a distance of 300 pc (the thin disk scale height), with 3σ or better geometric distances, trigonometric parallax measurements accurate to 1 mas are required. To achieve the required proper motion and parallax accuracy with an assumed astrometric accuracy of 10 mas per observation per coordinate, approximately 1,000 observations are required. This requirement on the number of observations is in good agreement with the independent constraint implied by the difference between the total depth and the single-visit depth.

2.1.5. A Summary and Synthesis of Science-driven Constraints on Data Properties

The goals of all the science programs discussed above (and many more, of course) can be accomplished by satisfying the following minimal constraints⁴⁰

⁴⁰ For a more elaborate listing of various constraints, including detailed specification of various probability distribu-

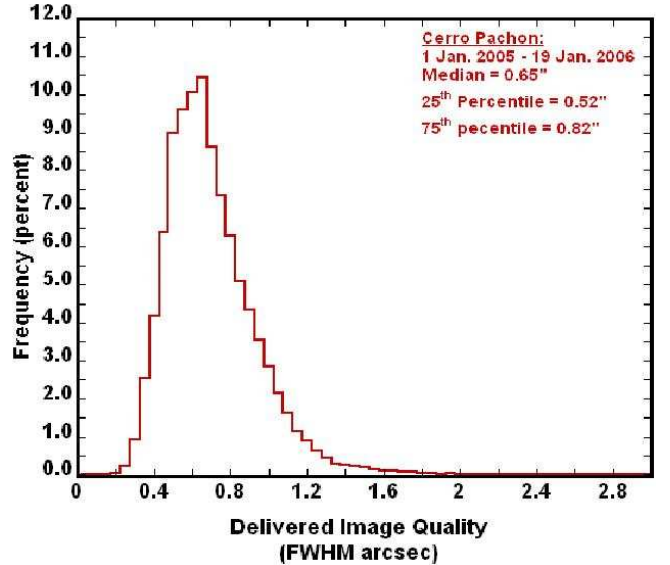


FIG. 1.— The image quality distribution measured at the Cerro Pachón site using a DIMM (differential image motion monitor) at $\lambda = 500$ nm, and corrected using an outer scale parameter of 30 m over an 8.4 m aperture. For details about the outer scale correction see Tokovinin (2002). The observed distribution is well described by a log-normal distribution, using the parameters shown in the figure.

1. *The single visit depth* should reach $r \sim 24.5$. This limit is primarily driven by the NEO survey and variable sources (e.g., SN, RR Lyrae stars), and by proper motion and trigonometric parallax measurements for stars. Indirectly, it is also driven by the requirements on the coadded survey depth and the minimum number of exposures placed by WL science.
2. *Image quality* should maintain the limit set by the atmosphere (the median free-air seeing is 0.7 arcsec in the r band at the chosen site, see Fig. 1), and not be degraded appreciably by the hardware. In addition to stringent constraints from weak lensing, good image quality is driven by the required survey depth for point sources and by image differencing techniques.
3. *Photometric repeatability* should achieve 5 mmag precision at the bright end, with zeropoint stability across the sky of 10 mmag and band-to-band calibration errors not larger than 5 mmag. These requirements are driven by the photometric redshift accuracy, the separation of stellar populations, detection of low-amplitude variable objects (such as eclipsing planetary systems), and the search for systematic effects in type Ia supernova light curves.
4. *Astrometric precision* should maintain the limit set by the atmosphere, of about 10 mas per visit at the bright end (on scales below 20 arcmin). This precision is driven by the desire to achieve a proper motion accuracy of 0.2 mas/yr and parallax accuracy of 1.0 mas over the course of a 10-year survey (see §2.2.1).

tions, please see the LSST Science Requirements Document (<http://www.lsst.org/Science/docs.shtml>).

5. *The single visit exposure time* (including both exposures in a visit) should be less than about a minute to prevent trailing of fast moving objects and to aid control of various systematic effects induced by the atmosphere. It should be longer than ~ 20 seconds to avoid significant efficiency losses due to finite readout, slew time, and read noise.
6. *The filter complement* should include at least six filters in the wavelength range limited by atmospheric absorption and silicon detection efficiency (320–1050 nm), with roughly rectangular filters and no large gaps in the coverage, in order to enable robust and accurate photometric redshifts and stellar typing. An SDSS-like u band is extremely important for separating low-redshift quasars from hot stars, and for estimating the metallicities of F/G main sequence stars. A bandpass with an effective wavelength of about 1 micron would enable studies of sub-stellar objects, high-redshift quasars (to redshifts of ~ 7.5), and regions of the Galaxy that are obscured by interstellar dust.
7. *The revisit time distribution* should enable determination of orbits of Solar System objects and sample SN light curves every few days, while accommodating constraints set by proper motion and trigonometric parallax measurements.
8. *The total number of visits* of any given area of sky, when accounting for all filters, should be of the order of 1,000, as mandated by WL science, the NEO survey, and proper motion and trigonometric parallax measurements. Studies of transient sources also benefit from a larger number of visits.
9. *The coadded survey depth* should reach $r \sim 27.5$, with sufficient signal-to-noise ratio in other bands to address both extragalactic and Galactic science drivers.
10. *The distribution of visits per filter* should enable accurate photometric redshifts, separation of stellar populations, and sufficient depth to enable detection of faint extremely red sources (e.g., brown dwarfs and high-redshift quasars). Detailed simulations of photometric redshift estimates suggest an approximately flat distribution of visits among bandpasses (because the system throughput and atmospheric properties are wavelength dependent, the achieved depths are different in different bands). The adopted time allocation (see Table 1) gives a slight preference to the r and i bands because of their dominant role in star/galaxy separation and weak lensing measurements.
11. *The distribution of visits on the sky* should extend over at least $\sim 20,000 \text{ deg}^2$ to obtain the required number of galaxies for WL studies, with attention paid to include “special” regions such as the Ecliptic, Galactic plane, and the Large and Small Magellanic Clouds.
12. *Data processing, data products and data access* should enable efficient science analysis without a significant impact on the final uncertainties. To

TABLE 1
THE LSST BASELINE DESIGN AND SURVEY PARAMETERS

Quantity	Baseline Design Specification
Optical Config.	3-mirror modified Paul-Baker
Mount Config.	Alt-azimuth
Final f-Ratio, aperture	f/1.234, 8.4 m
Field of view, étendue	9.6 deg ² , 318 m ² deg ²
Plate Scale	50.9 $\mu\text{m}/\text{arcsec}$ (0.2" pix)
Pixel count	3.2 Gigapix
Wavelength Coverage	320 – 1050 nm, <i>ugrizy</i>
Single visit depths ^a (5σ)	23.9, 25.0, 24.7, 24.0, 23.3, 22.1
Mean number of visits	70, 100, 230, 230, 200, 200
Final (coadded) depths ^a	26.3, 27.5, 27.7, 27.0, 26.2, 24.9

^a The listed values for 5σ depths in the *ugrizy* bands, respectively, are AB magnitudes, and correspond to point sources and zenith observations. See Table 2 for more details.

enable a fast and efficient response to transient sources, the processing latency should be less than a minute, with a robust and accurate preliminary classification of reported transients.

Remarkably, even with these joint requirements, none of the individual science programs is severely over-designed. That is, despite their significant scientific diversity, these programs are highly compatible in terms of desired data characteristics. Indeed, any one of the four main science drivers could be removed, and the remaining three would still yield very similar requirements for most system parameters. As a result, the LSST system can adopt a highly efficient survey strategy where *a single dataset serves most science programs* (instead of science-specific surveys executed in series). One can think of this as *massively parallel astrophysics*. The vast majority (about 90%) of the observing time will be devoted to a deep-wide-fast survey mode, with the remaining 10% of observing time allocated to special programs which will also address multiple science goals. Before describing these surveys in detail, we discuss the main system parameters.

2.2. The Main System Design Parameters

Given the minimum science-driven constraints on the data properties listed in the previous section, we now discuss how they are translated into constraints on the main system design parameters: the aperture size, the survey lifetime, the optimal exposure time, and the filter complement.

2.2.1. The Aperture Size

The product of the system’s étendue and the survey lifetime, for given observing conditions, determines the sky area that can be surveyed to a given depth, where the étendue is the product of the primary mirror area and the field-of-view area. The LSST field-of-view area is maximized to its practical limit, 10 deg², determined by the requirement that the delivered image quality be dominated by atmospheric seeing at the chosen site (Cerro Pachón in Northern Chile). A larger field-of-view would lead to unacceptable deterioration of the image quality. This leaves the primary mirror diameter and survey lifetime as free parameters. The adopted survey lifetime of 10 years is a compromise between a shorter time that

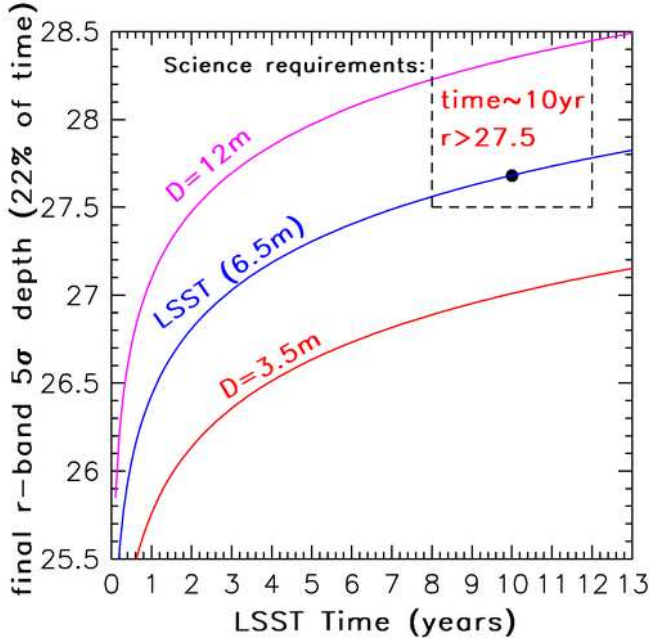


FIG. 2.— The coadded depth in the r band (AB magnitudes) vs. the effective aperture and the survey lifetime. It is assumed that 22% of the total observing time (corrected for weather and other losses) is allocated for the r band, and that the ratio of the surveyed sky area to the field-of-view area is 2,000.

leads to an excessively large and expensive mirror (15m for a 3 year-long survey and 12m for a 5-year long survey), and a smaller telescope that would require more time to complete the survey, with the associated increase in operations cost.

The primary mirror size is a function of the required survey depth and the desired sky coverage. By and large, the anticipated science outcome scales with the number of detected sources. For practically all astronomical source populations, in order to maximize the number of detected sources, it is more advantageous to maximize the area first, and then the detection depth⁴¹ For this reason, the sky area for the main survey is maximized to its practical limit, 20,000 deg², determined by the requirement to avoid large airmasses ($X < 1.5$, where $X = 1/\cos(\theta)$ and θ is the zenith distance), which would substantially deteriorate the image quality and the survey depth (see eq. 6).

With the adopted field-of-view area, the sky coverage and the survey lifetime fixed, the primary mirror diameter is fully driven by the required survey depth. There are two depth requirements: the final (coadded) survey depth, $r \sim 27.5$, and the depth of a single visit, $r \sim 24.5$. The two requirements are compatible if the number of visits is several hundred (per band), which is in good agreement with independent science-driven requirements on the latter.

⁴¹ If the exposure time is doubled and used to double the survey area, the number of sources increases by a factor of two. If the survey area is kept fixed, the increased exposure time will result in ~ 0.4 mag deeper data (see eq. 6). For cumulative source counts described by $\log(N) = C + k \cdot m$, the number of sources will increase by more than a factor of two only if $k > 0.75$. Apart from low-redshift quasars ($z < 2$), practically all populations have k at most 0.6 (the so-called Euclidean counts), and faint stars and galaxies have $k < 0.5$. For more details, please see Nemiroff (2003).

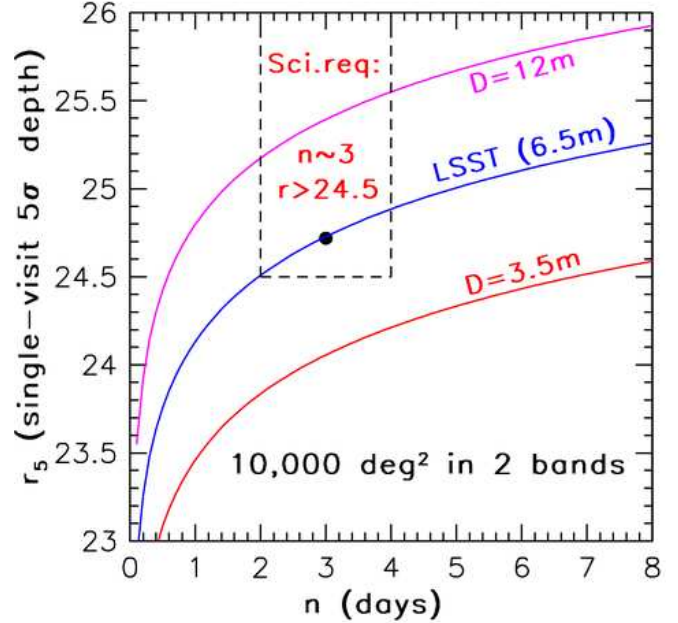


FIG. 3.— The single-visit depth in the r band (5σ detection for point sources, AB magnitudes) vs. revisit time, n (days), as a function of the effective aperture size. With a coverage of 10,000 deg² in two bands, the revisit time directly constrains the visit exposure time, $t_{vis} = 10n$ seconds. In addition to direct constraints on optimal exposure time, t_{vis} is also driven by requirements on the revisit time, n , the total number of visits per sky position over the survey lifetime, N_{visit} , and the survey efficiency, ϵ (see eqs. 1-3). Note that these constraints result in a fairly narrow range of allowed t_{vis} for the main deep-wide-fast survey.

The required coadded survey depth provides a direct constraint, independent of the details of survey execution such as the exposure time per visit, on the minimum effective primary mirror diameter of 6.5m, as illustrated in Fig. 2.

2.2.2. The Optimal Exposure Time

The single visit depth depends on both the primary mirror diameter and the chosen exposure time, t_{vis} . In turn, the exposure time determines the time interval to revisit a given sky position and the total number of visits, and each of these quantities has its own science drivers. We summarize these simultaneous constraints in terms of the single-visit exposure time:

- The single-visit exposure time should not be longer than about a minute to prevent trailing of fast Solar System moving objects, and to enable efficient control of atmospheric systematics.
- The mean revisit time (assuming uniform cadence) for a given position on the sky, scales as

$$n = \left(\frac{t_{vis}}{10 \text{ sec}} \right) \left(\frac{A_{sky}}{10,000 \text{ deg}^2} \right) \left(\frac{10 \text{ deg}^2}{A_{FOV}} \right) \text{ days}, \quad (1)$$

where two visits per night are assumed, and the losses for realistic observing conditions have been taken into account (with the aid of the Operations Simulator described below). Science drivers such as SN and moving objects in the Solar System require that $n < 4$ days, or equivalently $t_{vis} < 40$ seconds for the nominal values of A_{sky} and A_{FOV} .

- The number of visits to a given position on the sky, N_{visit} , with losses for realistic observing conditions taken into account, is given by

$$N_{visit} = \left(\frac{3000}{n} \right) \left(\frac{T}{10 \text{ yr}} \right). \quad (2)$$

The requirement $N_{visit} > 800$ again implies that $n < 4$ and $t_{vis} < 40$ seconds if the survey lifetime, $T \sim 10$ years.

- These three requirements place a firm upper limit on the optimal visit exposure time of $t_{vis} < 40$ seconds. Surveying efficiency (the ratio of open-shutter time to the total time spent per visit) considerations place a lower limit on t_{vis} due to finite read-out and slew time (the longest acceptable read-out time is set to 2 seconds, and the slew and settle time is set to 5 seconds, including the read-out time for the second exposure in a visit):

$$\epsilon = \left(\frac{t_{vis}}{t_{vis} + 9 \text{ sec}} \right). \quad (3)$$

To maintain efficiency losses below 30% (i.e., at least below the limit set by the weather patterns), and to minimize the read noise impact, $t_{vis} > 20$ seconds.

Taking these constraints simultaneously into account, as summarized in Fig. 3, yielded the following reference design:

1. A primary mirror effective diameter of $\sim 6.5\text{m}$. With the adopted optical design, described below, this effective diameter corresponds to a geometrical diameter of $\sim 8\text{m}$. Motivated by characteristics of the existing equipment at the Steward Mirror Laboratory, which is casting the primary mirror, the adopted geometrical diameter is set to 8.4m .
2. A visit exposure time of 30 seconds (using two 15 second exposures to efficiently reject cosmic rays), yielding $\epsilon = 77\%$.
3. A revisit time of 3 days on average per $10,000 \text{ deg}^2$ of sky, with two visits per night.

To summarize, the chosen primary mirror diameter is the *minimum* diameter that simultaneously satisfies the depth ($r \sim 24.5$ for single visit and $r \sim 27.5$ for coadded depth) and cadence (revisit time of 3-4 days, with 30 seconds per visit) constraints described above.

2.3. System Design Trade-offs

We note that the Pan-STARRS project (Kaiser et al. 2002), with similar science goals as LSST, has adopted a distributed aperture design, where the total system étendue is a sum of étendue values for an array of small telescopes (the prototype PS1 telescope has an étendue of $1/24^{\text{th}}$ of the LSST's étendue). Similarly, the LSST system could perhaps be made as two smaller copies with 6m mirrors, or 4 copies with 4m mirrors, or 16 copies with 2m mirrors. Each of these clones would have to have its own 3 Gigapixel camera (see below), and given the added risk and complexity (e.g., data processing),

the monolithic design seems advantageous for a system with such a large étendue as LSST.

It is informative to consider the tradeoffs that would be required for a system with a smaller aperture, if the science requirements were to be maintained. For this comparison, we consider a four-telescope version of the Pan-STARRS survey (PS4). With an étendue about 6 times smaller than that of LSST (effective diameters of 6.5m and 3.0m, and a field-of-view area of 9.6 deg^2 vs. 7.2 deg^2), and all observing conditions being equal, the PS4 system could in principle use an identical cadence as that of LSST. The main difference in the datasets would be a faint limit shallower by about 1 mag in a given survey lifetime. As a result, for Euclidean populations the sample sizes would go down by a factor of 4, while for shallower populations (e.g., galaxies around redshift of 1) the samples would be smaller by about a factor 2-3. The distance limits for nearby sources, such as Milky Way stars, would drop to 60% of their corresponding LSST values, and the NEO completeness level mandated by the U.S. Congress would not be reached.

If instead the survey coadded depth were to be maintained, then the survey sky area would have to be 6 times smaller ($\sim 3,500 \text{ deg}^2$). If the survey single-visit depth were to be maintained, then the exposure time would have to be about 6 times longer (ignoring the slight difference in the field-of-view area and simply scaling by the étendue ratio), resulting in non-negligible trailing losses for solar system objects, and either i) a factor of six smaller sky area observed within $n = 3$ days, or ii) the same sky area revisited every $n = 18$ days. Given these conflicts, one solution would be to split the observing time and allocate it to individual specialized programs (e.g., large sky area vs. deep coadded data vs. deep single-visit data vs. small n data, etc.), as considered by the PS1 Consortium⁴².

In summary, *given the science requirements as stated here, there is a minimum étendue of $\sim 300 \text{ deg}^2 \text{ m}^2$ which enables seemingly disparate science goals to be addressed with a single data set.* A system with a smaller étendue would require specialized surveys to address the science goals, which results in a loss of surveying efficiency⁴³. The LSST is designed to reach this minimum étendue for the science goals stated in its Science Requirements Document.

2.4. The Filter Complement

The LSST filter complement (*ugrizy*, see Fig. 4) is modeled after the Sloan Digital Sky Survey (SDSS) system (Fukugita et al. 1996) because of its demonstrated success in a wide variety of applications, including photometric redshifts of galaxies (Budavári et al. 2003), separation of stellar populations (Lenz et al. 1998; Helmi et al. 2003), and photometric selection of quasars (Richards et al. 2002). The extension of the SDSS system to longer wavelengths (the *y* band at ~ 1 micron) is driven by the increased effective redshift range achievable with the LSST due to deeper imaging, the desire to study sub-stellar objects, high-redshift quasars, regions of the

⁴² More information about Pan-STARRS is available from <http://pan-starrs.ifa.hawaii.edu>.

⁴³ The converse is also true: for every étendue there is a set of optimal science goals that such a system can address with a high efficiency.

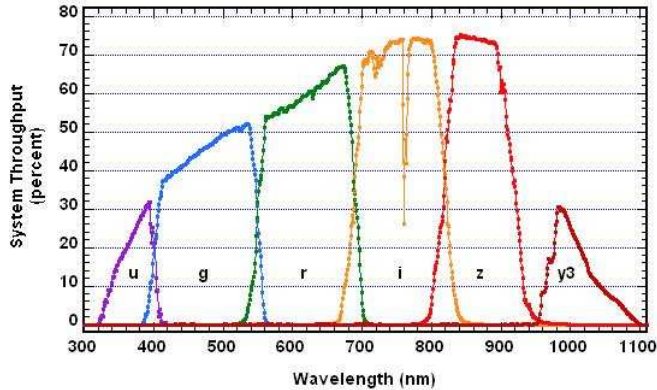


FIG. 4.— The *current* design of the LSST bandpasses. The vertical axis shows the total throughput. The computation includes the atmospheric transmission, optics, and the detector sensitivity. The detailed design of the *y* band is still being optimized and the figure shows the so-called *y*₃ version which avoids the atmospheric water absorption feature at $\sim 0.95 \mu\text{m}$.

Galaxy that are obscured by interstellar dust, and the scientific opportunity enabled by modern CCDs with high quantum efficiency in the near infrared.

The chosen filter complement corresponds to a design “sweet spot”. We have investigated the possibility of replacing the *ugrizy* system with a filter complement that includes only five filters. For example, each filter width could be increased by 20% over the same wavelength range (neither a shorter wavelength range, nor gaps in the wavelength coverage are desirable options), but this option is not satisfactory. Placing the red edge of the *u* band blueward of the Balmer break allows optimal separation of stars and quasars, and the telluric water absorption feature at 9500 Angstroms effectively defines the blue edge of the *y* band. Of the remaining four filters (*griz*), the *g* band is already quite wide. As a last option, the *riz* bands could be redesigned as two wider bands. However, this option is also undesirable because the *r* and *i* bands are the primary bands for weak lensing studies and for star/galaxy separation, and chromatic atmospheric refraction would worsen the point spread function for a wider bandpass.

2.5. The Calibration Methods

Precise determination of the point spread function across each image, accurate photometric and astrometric calibration, and continuous monitoring of system performance and observing conditions will be needed to reach the full potential of the LSST mission. Extensive precursor data including the massive SDSS dataset and our own data obtained using telescopes close to the LSST site of Cerro Pachón (e.g., the SOAR and Gemini South telescopes), as well as telescopes of similar aperture (e.g., Subaru), indicate that the photometric and astrometric accuracy will be limited not by our instrumentation or software, but rather by atmospheric effects. Active optics will assure superb image quality.

The required 1% photometric accuracy is driven by our requirements on the photometric redshift accuracy, the separation of stellar populations, the ability to detect low-amplitude variable objects, and the search for systematic effects in type Ia supernova light curves. SDSS data taken in good photometric conditions have indeed reached the LSST requirements (Padmanabahn et al.

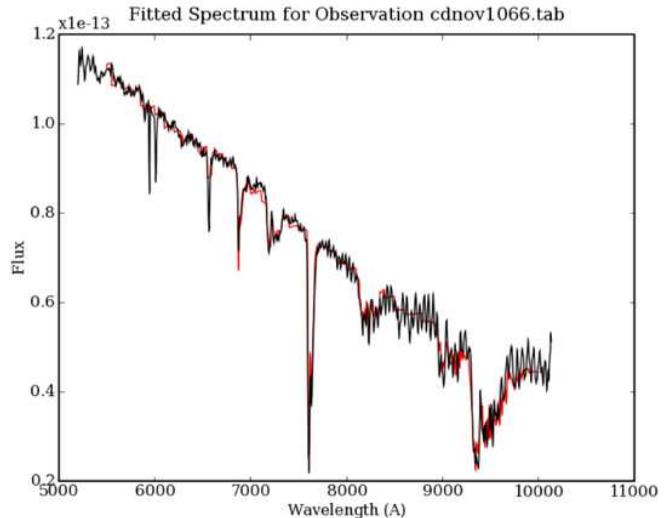


FIG. 5.— An example of determination of the atmospheric opacity by simultaneously fitting a 3-parameter stellar model SED (Kurucz 1979) and six physical parameters of a sophisticated atmospheric model (MODTRAN, Anderson et al. 1999) to an observed F-type stellar spectrum (F_λ). The black line is the observed spectrum and the red line is the best fit. Note that the atmospheric water feature around $0.9\text{--}1.0 \mu\text{m}$ is exquisitely well fit. The components of the best-fit atmospheric opacity are shown in Fig. 6. Adapted from Burke et al. (2007).

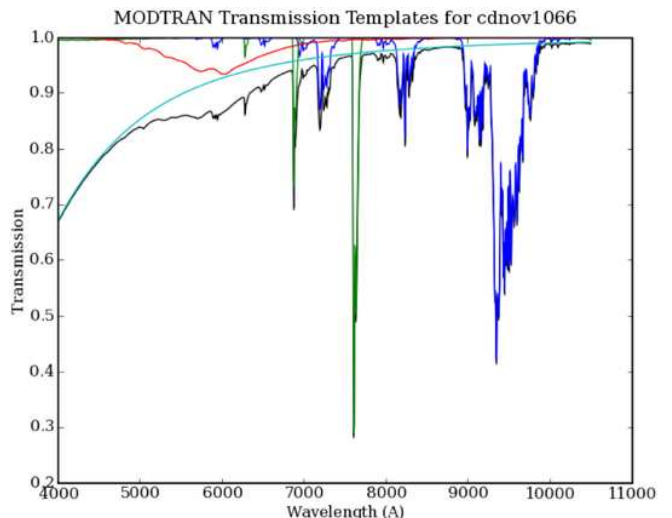


FIG. 6.— The components of the best-fit atmospheric opacity used to model the observed stellar spectrum shown in Fig. 5. The atmosphere model (MODTRAN, Anderson et al. 1999) includes six components: water vapor (blue), oxygen and other trace molecules (green), ozone (red), Rayleigh scattering (cyan), a gray term with a transmission of 0.989 (not shown) and an aerosol contribution proportional to λ^{-1} and extinction of 1.3% at $\lambda=0.675 \mu\text{m}$ (not shown). The black line shows all six components combined. Adapted from Burke et al. (2007).

2008), though measurements with ground-based telescopes typically produce data with errors a factor of two or so larger. Analysis of repeated SDSS scans obtained in varying observing conditions demonstrates that data obtained in traditionally non-photometric conditions can also be calibrated with sufficient accuracy (Ivezić et al. 2007b).

The LSST calibration plan builds on experience gained from the SDSS survey. The process decouples the establishment of a stable and uniform internal relative calibra-

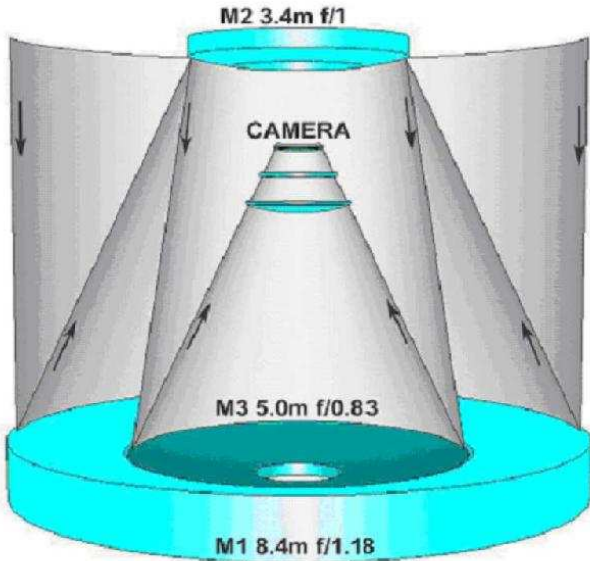


FIG. 7.— The LSST baseline optical design with its unique monolithic mirror: the primary and tertiary mirrors are positioned such that they form a continuous compound surface, allowing them to be polished into a single substrate.

tion from the task of assigning absolute optical flux to celestial objects. The latter task requires determination of a small number of factors appropriate for the accumulated multi-epoch data set. Celestial sources will be used to define the internal photometric system and to monitor stability and uniformity of photometric data. There will be >100 main-sequence stars with $17 < r < 20$ per detector (14×14 arcmin²) even at high Galactic latitudes. Standardization of photometric scales will be achieved through direct observation of stars with well-understood spectral energy distributions (SEDs).

While the primary source of data used for photometric calibration will be science images taken with the main telescope, these images alone will be insufficient to fully characterize instrumental and atmospheric temporal and spatial variations that can affect photometric measurements. Auxiliary instrumentation, including a 1.5m calibration telescope will provide the calibration parameters needed for image processing, to calibrate the instrumental response of the LSST hardware (Stubbs & Tonry 2006), and to measure the atmospheric optical depth as a function of wavelength along the LSST line of sight (Stubbs et al. 2007; see Figs. 5 and 6).

2.6. The LSST Reference Design

We briefly describe the reference design for the main LSST system components. Detailed discussion of the flow-down from science requirements to system design parameters, and extensive system engineering analysis can be found in Claver et al. (2008, in prep.).

2.6.1. Telescope and Site

The large LSST étendue is achieved in a novel three-mirror design (modified Paul-Baker; Angel, Lesser & Sarlot 2000) with a very fast f/1.234 beam. The optical design has been optimized to yield a large field of view (9.6 deg²), with seeing-limited image quality, across a wide



FIG. 8.— The baseline design (modified three-mirror Paul-Baker) for the LSST telescope (current since April 2006).

wavelength band (320–1050 nm). Incident light is collected by the primary mirror, which is an annulus with an outer diameter of 8.4 m (an effective diameter of 6.5m), then reflected to a 3.4m convex secondary, onto a 5m concave tertiary, and finally into three refractive lenses in a camera (see Fig. 7). This is achieved with an innovative approach that positions the tertiary mirror inside the primary mirror annulus ring, making it possible to fabricate the mirror pair from a single monolithic blank using borosilicate technology. The secondary will be a thin meniscus mirror, fabricated from an ultra-low expansion material. All three mirrors will be actively supported to control wavefront distortions introduced by gravity and environmental stresses on the telescope.

The telescope mount is a compact, stiff structure with a fundamental frequency of nearly 10 Hz, which is crucial for achieving the required fast slew-and-settle times (see Fig. 8). The telescope sits on a concrete pier within a carousel dome that is 30 m in diameter (Fig. 9). The dome has been designed to reduce dome seeing (local air turbulence that can distort images) and to maintain a uniform thermal environment over the course of the night. The LSST Observatory will be sited atop Cerro Pachón in northern Chile, near the Gemini South and SOAR telescopes (latitude: S $30^\circ 10' 20.1''$; longitude: W $70^\circ 48' 0.1''$; elevation: 2123 m; the median r band zenith seeing: 0.7 arcsec).

2.6.2. Camera

The LSST camera provides a 3.2 Gigapixel flat focal plane array, tiled by 189 $4K \times 4K$ CCD science sensors with $10 \mu\text{m}$ pixels (see Figs. 10 and 11). This pixel count is a direct consequence of sampling the 9.6 deg² field-of-view (0.64m diameter) with 0.2×0.2 arcsec² pixels (Nyquist sampling in the best expected seeing of ~ 0.4 arcsec). The sensors are deep depleted, back-illuminated devices with a highly segmented architecture that enables the entire array to be read in 2 seconds. The detectors are grouped into 3×3 rafts (see Fig. 12), each containing its own dedicated front-end and back-end electronics boards. The rafts are mounted on a silicon carbide grid inside a vacuum cryostat, with an intricate thermal control system that maintains the CCDs at an operating temperature of 180 K. The entrance window to the



FIG. 9.— The LSST Observatory: artist's rendering of the dome enclosure with the attached summit support building and the LSST calibration telescope shown on an adjacent peak (Michael J. Mullen Design).

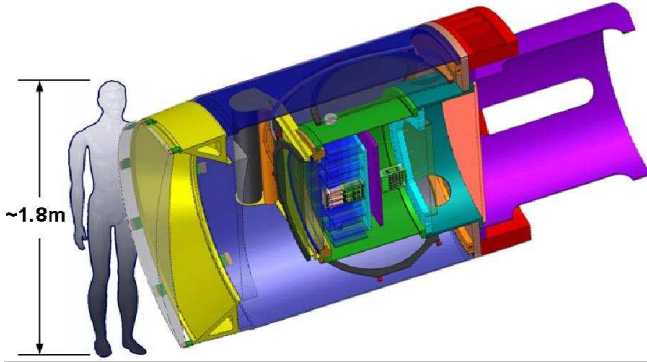


FIG. 10.— The LSST camera with a person to indicate scale size. The camera is positioned in the middle of the telescope and will include a filter mechanism and shuttering capability.

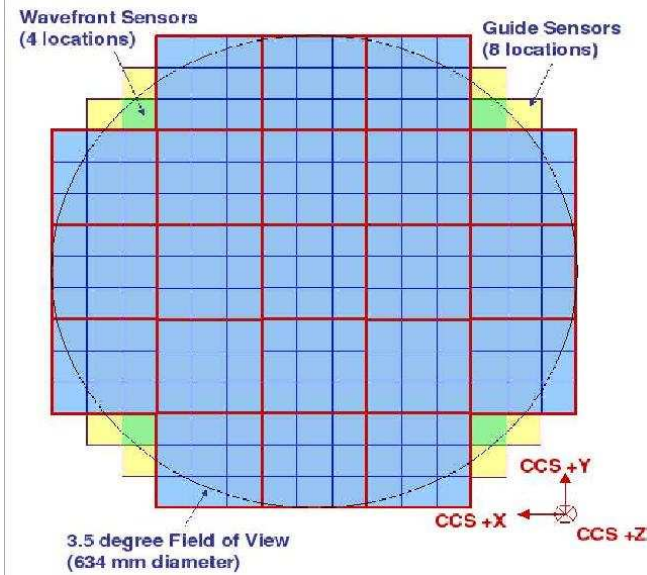


FIG. 11.— The LSST focal plane. Each cyan square represents one 4096×4096 pixel sensor. Nine sensors are assembled into a raft; the 21 rafts are outlined in red. There are 189 science sensors, each with 16.8 Mpix, for a total pixel count of 3.2 Gpix.

cryostat is the third of the three refractive lenses in the camera. The other two lenses are mounted in an optics structure at the front of the camera body, which also contains a mechanical shutter, and a carousel assembly

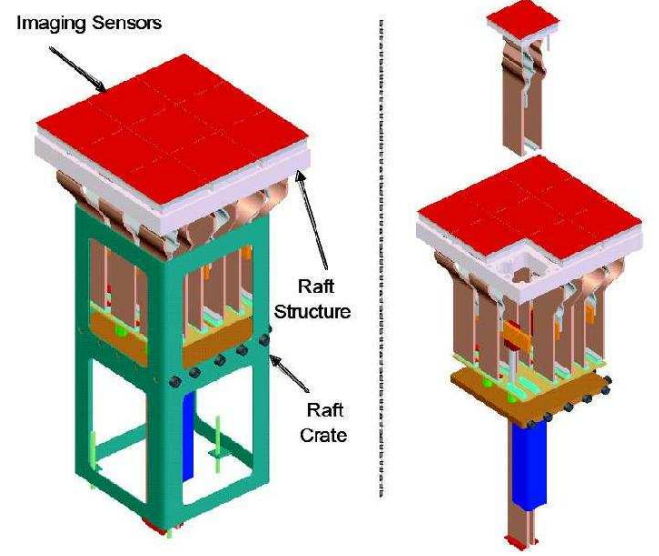


FIG. 12.— The LSST raft module with integrated front-end electronics and thermal connections. Each raft includes 9 sensors and can be replaced on a short timescale.

Data Products Source Catalog, Object Catalog, Images, Alerts		Pipelines Image Processing, Detection, Association, Moving Object, Classification, Calibration
Application Framework Image, Astronomical Object, Catalog, Collection, Table, Meta-Data, Component, Processing Stage, Processing Slice		
Data Access Data Access Framework, Distributed File System, Database Management System	User Interface Data Quality Visualization, VO Interfaces	Distributed Processing Pipeline Construction, Pipeline Execution, Management and Control
System Administration, Operations, Security System Resource Management, User Management, Certificate-based Security		
Computing Clusters/Servers, Operating System	Storage Disk, Tape, Controllers, Storage Management Software	Communications Fiber, Switches, Routers, Firewalls, Communications Stacks, Network Management Software
Physical Plant Power, Cooling, Space		

FIG. 13.— The three-layered architecture of the data management system (application, middleware and infrastructure layers) enables scalability, reliability, and evolutionary capability.

that holds five large optical filters. A sixth optical filter will also be fabricated and can replace any of the five via a procedure accomplished during daylight hours.

2.6.3. Data Management

The rapid cadence of the LSST observing program will produce an enormous volume of data, ~ 30 TB per night, leading to a total database over the ten years of operations of 60 PB for the raw data, and 30 PB for the catalog database. The total data volume after processing will be several hundred PB, processed using ~ 100 TFlops of computing power. Processing such a large volume of data, converting the raw images into a faithful representation of the Universe, automated data quality assessment, and archiving the results in useful form for a broad community of users is a major challenge.

The data management system is configured in three levels: an infrastructure layer consisting of the comput-

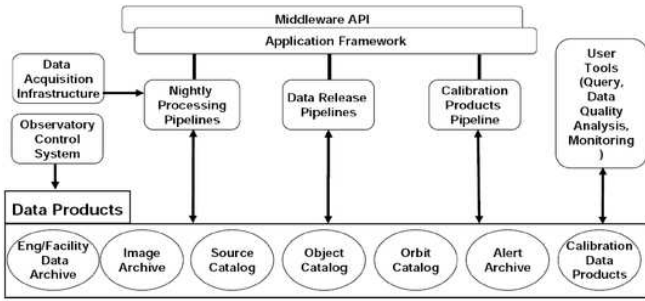


FIG. 14.— The application layer of the data management system. The arrows indicate direction of the data flow. The main pipelines enable nightly processing, calibration, and data releases

ing, storage, and networking hardware and system software; a middleware layer, which handles distributed processing, data access, user interface, and system operations services; and an applications layer, which includes the data pipelines and products and the science data archives (see Fig. 13). The application layer (see Fig. 14) is organized around the data products being produced. The nightly pipelines (see Fig. 15) are based on image subtraction, and are designed to rapidly detect interesting transient events in the image stream and send out alerts to the community within 30 seconds from completing the image readout. The data release pipelines (see Fig. 16), in contrast, are intended to produce the most completely analyzed data products of the survey, in particular those that measure very faint objects and cover long time scales. A new run begins each year, processing the entire survey data set that is available. The data release pipelines consume most of the computing power of the data management system. The calibration products pipeline produces the wide variety of calibration data required by the other pipelines. All of these pipelines are architected to make efficient use of linux clusters with thousands of nodes.

There will be both mountain summit and base computing facilities, as well as a central archive facility and multiple data access centers. The data will be transported over existing high-speed optical fiber links from South America to the U.S. (see Fig. 17). Although the data processing center will have substantial computing power (~ 100 TFlops, equal to the world's most powerful computer in 2004), the continuation of current trends suggests that it will not even qualify for the top 500 list by the time of first light in 2014. Hence, while LSST is making a novel use of advances in information technology, it is not taking the risk of pushing the expected technology to the limit.

3. ANTICIPATED DATA PRODUCTS AND THEIR CHARACTERISTICS

The LSST observing strategy is designed to maximize the scientific throughput by minimizing slew and other downtime and by making appropriate choices of the filter bands given the real-time weather conditions. We first describe a simulator that has been developed to evaluate this process and then illustrate with two examples how its outputs have been used to predict LSST performance.

3.1. The LSST Operations Simulator

The LSST Operations Simulator was developed to enable a detailed quantitative analysis of the various science

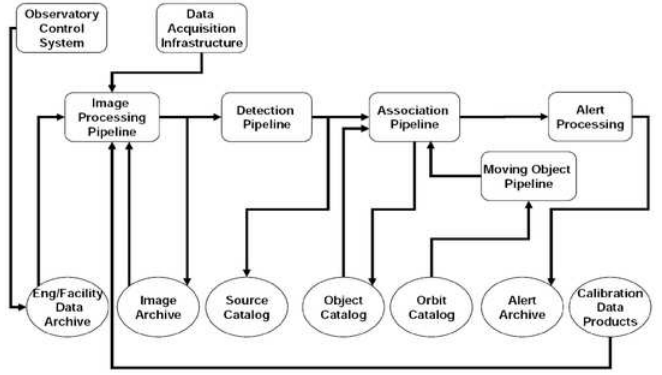


FIG. 15.— The structure of nightly pipelines. Their main task is to compare new data to the previously accumulated data and search for transient, variable and moving objects.

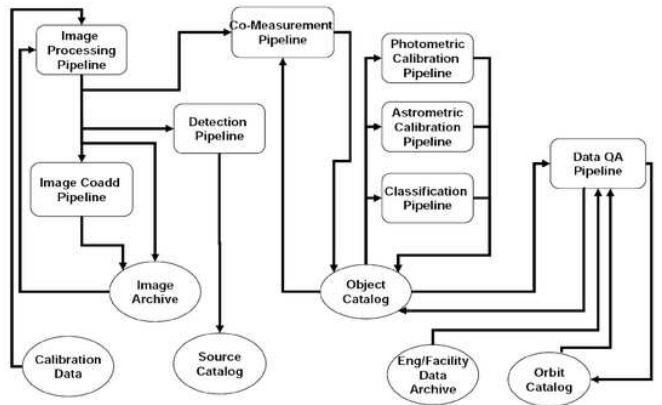


FIG. 16.— The structure of data release pipelines. These pipelines are intended to produce the most completely analyzed data products of the survey, and will consume most of the computing power of the data management system.



FIG. 17.— The LSST data flow from the mountain summit/base facility in Chile to the data access center and archive centers in the U.S.

tradeoffs described in this paper. It contains detailed models of site conditions, hardware and software performance, and an algorithm for scheduling observations which will, eventually, drive the largely robotic observatory. Observing conditions include a model for seeing derived from an extensive body of on-site MASS/DIMM (Multi-Aperture Scintillation Sensor and Differential Image Motion Monitor) measurements obtained during site selection and characterization (see Fig. 1). It not only

reproduces the observed seeing distribution, but includes the auto-correlation spectrum of seeing with time over intervals from minutes to seasons. Weather data are taken from ten years of hourly measurements at nearby Cerro Tololo. The time history of site conditions is important if the simulation is to faithfully reproduce a sequence of observations. Thus, for example, the simulator correctly represents the variation of limiting magnitude between pairs of observations used to detect NEOs and the correlation between, for example, seasonal weather patterns and observing conditions at any given point on the sky. The signal-to-noise ratio of each observation is determined using a sky background model which includes the dark sky brightness in each filter, the effects of seeing and atmospheric transparency, and a detailed model for scattered light from the moon and/or twilight at each observation. The time taken to move from one observation to the next is given by a detailed model of the camera, telescope, and dome. It includes such effects as the acceleration/deceleration profiles employed in moving in altitude, azimuth, camera rotator, dome azimuth, and wind/stray light screen altitude, the time taken to damp vibrations excited by each slew, cable wrap, time taken for active optics lock and correction as a function of slew distance, filter change, and focal plane readout.

Observations are scheduled by a ranking algorithm. After a given exposure, all possible next observations are assigned a score which depends upon their locations, times, and filters according to a set of scientific requirements which can vary with time and location. For example, if an ecliptic field has been observed in the r band, the score for another r -band observation of the same field will initially be quite low, but it will rise in time to peak about an hour after the first observation, and decline thereafter. This results in these observations being acquired as pairs roughly an hour apart, which enables efficient association of NEO detections. To ensure uniform sky coverage, fields with fewer previous observations will be scored more highly than those which have already been observed more frequently.

Once all possible next observations have been scored for scientific priority, their scores are modified according to observing conditions (e.g., seeing, airmass, and sky brightness) and to criteria such as low slew time to move from the current position, time spent to change filters, etc. The highest-ranked observation is then performed, and the cycle repeats. The result of a simulator run is a detailed history of which locations on the sky were observed when, in what filter, and with what sky background, seeing and other observing conditions. It takes about a week to produce a decade-long simulation using an average PC.

3.2. The Baseline LSST Surveys

The fundamental basis of the LSST concept is to scan the sky deep, wide, and fast, and to obtain a dataset that simultaneously satisfies the majority of the science goals. This concept, the so-called “universal cadence”, will yield the main deep-wide-fast survey (typical single visit depth of $r \sim 24.5$) and use about 90% of the observing time. The remaining 10% of observing time will be used to obtain improved coverage of parameter space such as very deep ($r \sim 26$) observations, observations with very short revisit times (~ 1 minute), and observa-

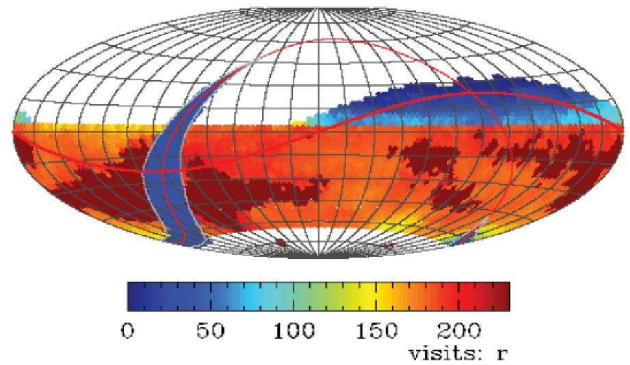


FIG. 18.— The distribution of the r band visits on the sky for one simulated realization of the baseline main survey. The sky is shown in Aitoff projection in equatorial coordinates and the number of visits for a 10-year survey is color-coded according to the inset. The two regions with smaller number of visits than the main survey (“mini-surveys”) are the Galactic plane (arc on the left) and the so-called “northern Ecliptic region” (upper right). The region around the South Celestial Pole will also receive substantial coverage (not shown here).

tions of “special” regions such as the Ecliptic, Galactic plane, and the Large and Small Magellanic Clouds. We are also considering a third type of survey, micro-surveys, that would use about 1% of the time (which still represents 25 nights on a unique 8m-class telescope).

3.2.1. The Main Deep-Wide-Fast Survey

The observing strategy for the main survey will be optimized for the homogeneity of depth and number of visits. In times of good seeing and at low airmass, preference is given to r -band and i -band observations. As often as possible, each field will be observed twice, with visits separated by 15-60 minutes. This strategy will provide motion vectors to link detections of moving objects in the Solar System, and fine-time sampling for measuring short-period variability. The ranking criteria also ensure that the visits to each field are widely distributed in position angle on the sky and rotation angle of the camera in order to minimize systematic effects in galaxy shape determination.

The universal cadence provides most of LSST’s power for detecting Near Earth Objects (NEO) and naturally incorporates the southern half of the ecliptic within its 20,000 square degrees (the northern half lies above the desired airmass limits, $X \lesssim 1.5$). NEO survey completeness for the smallest bodies (~ 140 m in diameter, per the Congressional NEO mandate) is greatly enhanced, however, by the addition of a crescent on the sky within 10 degrees of the northern ecliptic (see Fig. 18). Thus, the “northern Ecliptic proposal” extends the universal cadence to this region using the r and i filters only, along with more relaxed limits on airmass and seeing. Relaxed limits on airmass and seeing are also adopted for ~ 700 deg² around the south celestial pole, allowing coverage of the Large and Small Magellanic Clouds.

Finally, the universal cadence proposal excludes observations in a region of 1,000 square degrees around the Galactic Center, where the high stellar density leads to a confusion limit at much brighter magnitudes than those attained in the rest of the survey. Within this region, the Galactic Center proposal provides 30 observations in each of the six filters, distributed roughly logarithmically

in time (it may not be necessary to use the bluest u and g filters for this heavily extincted region).

The resulting sky coverage for the LSST baseline cadence, based on detailed operations simulations, is shown for the r band in Fig. 18. The anticipated total number of visits for a ten-year LSST survey is about 2.8 million (~ 5.6 million 15-second long exposures). The per-band allocation of these visits is shown in Table 1.

3.2.2. Mini-surveys

Although the uniform treatment of the sky provided by the universal cadence proposal can satisfy the majority of LSST scientific goals, roughly 10% of the time will be allocated to other strategies that significantly enhance the scientific return. These surveys aim to extend the parameter space accessible to the main survey by going deeper or by employing different time/filter sampling.

As an example of a mini-survey, consider a program that uses one hour of observing time per night to observe a relatively small region of sky to substantially greater depth in individual visits. Accounting for read-out time and filter changes, it could obtain about 50 consecutive 15-second exposures in each of four filters in an hour. If a field is visited every two days over four months, about 600 deg^2 can be observed with this cadence over 10 years. Taking weather into account, the selected fields would each have on average about 40 hour-long sequences of 200 exposures each. Each observation in a sequence would have an equivalent $5\text{-}\sigma$ depth of $r \sim 24$, and each filter subsequence when coadded would be 2 magnitudes deeper than the main survey visits ($r \sim 26.5$). When all 40 sequences and the main survey visits are coadded, they would extend the depth to $r \sim 28$.

This data set would be excellent for a wide variety of science programs. The individual sequences would be sensitive to 1% variability on hourly time scales, allowing discovery of planetary eclipses. If these fields were selected at Galactic latitudes of $|b| \sim 30 \text{ deg}$, they would include about 10 million stars observed with signal-to-noise ratio above 100 in each visit (stars brighter than $r \sim 21$). When subsequences from a given night were coadded, they would provide dense time sampling to a faint limit (in 4 bands, every 2 days over 120 days, modulo weather, to $r \sim 26.5$), and thus enable deep searches for SN, trans-Neptunian objects, and other faint transient, moving and variable sources. For example, the SN sample would be extended to redshifts of $z \sim 1.2$, with more densely sampled light curves than obtained from the universal cadence. Such sequences would also serve as excellent tests of our calibration procedures.

The baseline universal cadence is by no means the definitive plan for the entire survey. Rather, it represents a proof of concept that it is indeed possible to design a universal cadence which addresses a wide variety of science goals in a nearly optimal way. We are undertaking a vigorous and systematic research effort to explore the enormously large parameter space of possible surveys. The commissioning period will be used to test the usefulness of various observing modes and to explore alternative strategies. Proposals from the community, through the science collaborations (see § 5), for specialized cadences (such as mini-surveys and micro-surveys) will also be considered.

TABLE 2
THE PARAMETERS FROM EQS. 5 AND 6

	u	g	r	i	z	y
m_{sky}^a	21.8	22.0	21.3	20.0	19.1	17.5
θ^b	0.77	0.73	0.70	0.67	0.65	0.63
γ^c	0.037	0.038	0.039	0.039	0.040	0.040
C_m^d	23.60	24.57	24.57	24.47	24.19	23.74
k_m^e	0.48	0.21	0.10	0.07	0.06	0.06
m_5^f	23.9	25.0	24.7	24.0	23.3	22.1
Δm_5^g	0.21	0.16	0.14	0.13	0.13	0.13

^a The expected median zenith sky brightness at Cerro Pachón, assuming mean solar cycle and 3-day old moon (mag/arcsec^2).

^b The expected delivered median zenith seeing (arcsec). For larger airmass, X , seeing is proportional to $X^{0.6}$.

^c The band-dependent parameter from Eq. 5.

^d The band-dependent parameter from Eq. 6.

^e Adopted atmospheric extinction.

^f The typical 5σ depth for point sources at zenith, assuming exposure time of $2 \times 15 \text{ sec}$, and observing conditions as listed. For larger airmass the 5σ depth is brighter; see the bottom row.

^g The loss of depth at the median airmass of $X = 1.2$ due to seeing degradation and increased atmospheric extinction.

3.3. Detailed Analysis of Simulated Surveys

As examples of analysis enabled by the Operations Simulator, we describe determination of the completeness of the LSST NEO survey, and estimation of errors expected for trigonometric parallax and proper motion measurements. In both examples, the conclusions crucially depend on assumed signal-to-noise ratios, described next.

3.3.1. Expected Signal-to-Noise Ratio

The output of operations simulations is a data stream consisting of a position on the sky and the time of observation, together with observing conditions such as seeing and sky brightness. The expected photometric error (the inverse of signal-to-noise ratio) for a single visit can be written as

$$\sigma_1^2 = \sigma_{\text{sys}}^2 + \sigma_{\text{rand}}^2, \quad (4)$$

where σ_{rand} is the random photometric error and σ_{sys} is the systematic photometric error (includes errors due to, e.g., imperfect modeling of the point spread function, but does not include errors in absolute photometric zeropoint). The calibration system and procedures are designed to maintain $\sigma_{\text{sys}} < 0.005 \text{ mag}$. Based on SDSS experience (Sesar et al. 2007), the random photometric error, as a function of magnitude, is well described⁴⁴ by

$$\sigma_{\text{rand}}^2 = (0.04 - \gamma) x + \gamma x^2 \text{ (mag}^2\text{)}, \quad (5)$$

with $x = 10^{0.4(m-m_5)}$. Here m_5 is the 5σ depth (for point sources) in a given band, and γ depends on the sky brightness, readout noise, etc. Using the LSST exposure time calculator⁴⁵ (Gee et al. 2007), we have obtained the values of γ listed in Table 2. The 5σ depth for point sources is determined from

$$m_5 = C_m + 0.50 (m_{\text{sky}} - 21) + 2.5 \log_{10}(0.7/\theta) + 1.25 \log_{10}(t_{\text{vis}}/30) - k_m(X - 1) \quad (6)$$

⁴⁴ Eq. 5 can be derived from $\sigma_{\text{rand}} = N/S$, where N is noise and S is signal, and by assuming that $N^2 = N_o^2 + \alpha S$. The constants N_o and α can be expressed in terms of a single unknown constant γ by using the condition that $\sigma_{\text{rand}} = 0.2$ for $m = m_5$.

⁴⁵ Available at <http://dls.physics.ucdavis.edu/etc>.

where m_{sky} is the sky brightness (mag/arcsec²), θ is the seeing (FWHM, in arcsec), t_{vis} is the exposure time (seconds), k is the atmospheric extinction coefficient, and X is airmass. The constants C_m depend on the overall throughput of the instrument and are determined using the LSST exposure time calculator. The assumptions built into the calculator were tested using SDSS observations⁴⁶, and by comparing the predicted depths to the published performance of the Subaru telescope (Kashikawa et al. 2003). The adopted values for C_m and k are listed in Table 2, as well as expected m_5 in nominal observing conditions.

3.3.2. The NEO Completeness Analysis

To assess the LSST completeness for NEOs (more precisely, for a 20% subset of NEOs, the potentially hazardous asteroids or PHAs), the PHA population is represented by a size-limited complete sample of 800 true PHAs whose orbital elements are taken from the Minor Planet Center. The simulated baseline survey is used to determine which PHAs are present in each exposure and at what signal-to-noise ratio they were observed. In addition to seeing, atmospheric transparency, and sky background effects (see eq. 6), the signal-to-noise computation takes into account losses due to non-optimal filters and object trailing. Using SDSS observations of asteroids (Ivezić et al. 2001), we adopt the following mean colors to transform limiting (AB) magnitudes in LSST bandpasses (listed in Table 2) to an ‘effective’ limiting magnitude in the standard V band: $V - m = (-2.1, -0.5, 0.2, 0.4, 0.6, 0.6)$ for $m = (u, g, r, i, z, y)$. Due to very red $V - u$ colors, and the relatively bright limiting magnitude in the y band, the smallest objects are preferentially detected in the *griz* bands. The correction for trailing is implemented by subtracting from the right-hand side of eq. 6

$$\Delta m_5^{\text{trailing}} = 1.25 \log_{10}(1 + 0.0267 \frac{v t_{vis}}{\theta}), \quad (7)$$

where the object’s velocity, v , is expressed in deg/day. For the nominal exposure time of 30 seconds and $\theta = 0.7$ arcsec, the loss of limiting magnitude is 0.16 mag for $v = 0.25$ deg/day, typical for objects in the main asteroid belt, and 0.50 mag for $v = 1.0$ deg/day, typical of NEOs passing near Earth.

Above 60% completeness, one magnitude of depth is roughly equivalent to 10% in completeness. An object’s orbit is considered to be cataloged if the object was detected on at least three nights during a single lunation, with a minimum of two visits per night. The same criterion was used in NASA studies⁴⁷, and is confirmed as reliable by a detailed analysis of orbital linking and determination using the MOPS code (Jedicke et al. 2005) developed by the Pan-STARRS project (and adopted by

⁴⁶ SDSS data typically reach a 5σ depth for point sources of $r = 22.5$ with an effective aperture of $D = 2.22$ m, an exposure time of $t_{vis} = 54$ sec, the median r band sky brightness of $r_{sky} = 20.9$ mag/arcsec², the median seeing of $\theta = 1.5$ arcsec, and the median airmass of $X = 1.3$. In comparison, the LSST loss of depth is 0.32 mag due to shorter exposures, while the gains are 1.17 mag due to larger aperture, 0.83 mag due to better seeing, 0.20 mag due to fainter sky, and 0.10 mag due to better throughput, for the net gain of ~ 2.0 mag.

⁴⁷ The NASA 2007 NEO study is available from <http://neo.jpl.nasa.gov/neo/report2007.html>.

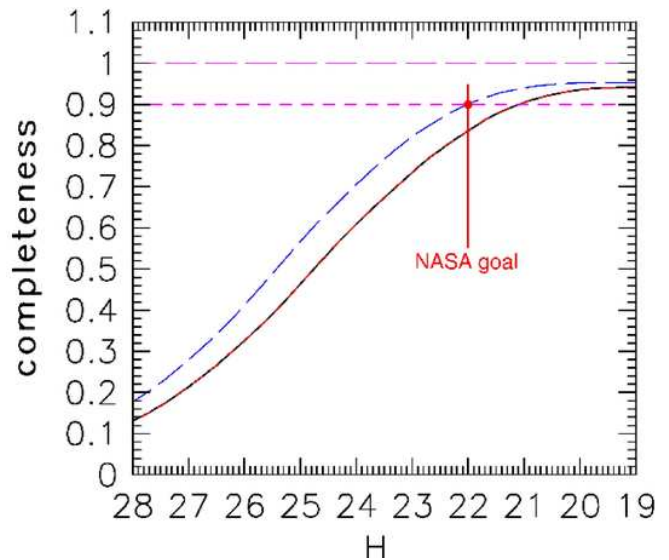


FIG. 19.— Completeness of the LSST survey for PHAs brighter than a given absolute magnitude (related to the size of the object and albedo; $H=22$ mag is equivalent to a typical 140m asteroid and $H=24$ mag is equivalent to a 50m asteroid). Two scenarios are shown: the lower curve is the 10-year long baseline survey with a 5% NEO optimization, and it reaches a completeness of 84%. The upper dashed curve results from spending 15% of the observing time in an NEO optimized mode, and running the survey for 12 years. It meets the 90% completeness level for 140m objects mandated by the Congress.

LSST in a collaborative effort with Pan-STARRS). The MOPS software system and its algorithms are significantly more advanced than anything fielded for this purpose to date. Realistic MOPS simulations show $>99\%$ linking efficiency across all classes of solar system objects. For the LSST baseline cadence, objects counted as cataloged are observed on 20 different nights on average over ten years. A more stringent requirement that an object must be detected on at least five nights decreases the completeness by typically 3%. The completeness is also a function of the assumed size distribution of NEOs: the flatter the distribution, the higher the completeness. If the latest results for the NEO size distribution by A. Harris (priv. comm.) are taken into account, the completeness increases by 1-2%. Due to these issues, the completeness estimates have a systematic uncertainty of at least 2%.

The LSST baseline cadence provides orbits for 82% of PHAs larger than 140 meters after 10 years of operations. With a minor change of this cadence, such as requiring that all observations in the so-called NE region (North Ecliptic region, defined by $\delta > 5^\circ$) are obtained in the r band, the completeness for 140m and larger PHAs is 84%, with 90% completeness reached for 200m and larger objects. The completeness curve as a function of an object’s size is shown in Fig. 19 (lower curve). This cadence spends 5% of the total observing time on NEO-optimized observations in the NE region.

Various adjustments to the baseline cadence can boost the completeness for 140m and larger PHAs to 90%. We find that such variations can have an unacceptably large impact on other science programs, if the 90% completeness is to be reached within the 10 year survey lifetime. However, with a minor adjustment of the baseline cadence, such that 15% of the time is spent in the NE region to reach fainter limiting magnitudes, this complete-

ness level can be reached with a 12-year long survey, and with a negligible effect on other science goals. The completeness curve as a function of an object's size for such a modified cadence is shown in Fig. 19 (upper curve).

Our analysis assumes that no NEOs are known prior to LSST. Currently known NEOs do not have a significant impact on this calculation. However, if a precursor survey, such as Pan-STARRS 4, operated for three years prior to LSST, the time to fulfill the Congressional mandate by LSST could be shortened by about a year (the current completeness level does not have a significant impact).

3.3.3. The Expected Accuracy of Trigonometric Parallax and Proper Motion Measurements

Given the observing sequence for each sky position in the main survey, we generate a time sequence of mock astrometric measurements. The assumed astrometric accuracy is a function of signal-to-noise ratio, SNR . Random astrometric errors per visit are modeled as θ/SNR , with $\theta = 700$ mas and SNR determined using eq. 6. The estimated proper motion and parallax accuracy at the bright end ($r < 20$) is driven by systematic errors due to the atmosphere. Systematic errors of 10 mas are added in quadrature, and are assumed to be *uncorrelated* between different observations of a given object. Systematic and random errors become similar at about $r = 22$, and there are about 100 stars per LSST sensor (0.05 sq. deg) to this depth (and fainter than the LSST saturation limit at $r \sim 16$) even at the Galactic poles.

Precursor data from the Subaru telescope indicate that systematic errors of 10 mas on spatial scales of several arcmins are realistic. Even a drift-scanning survey such as SDSS delivers uncorrelated systematic errors (dominated by seeing effects) at the level of 20-30 mas (measured from repeated scans, Pier et al. 2003), and the expected image quality for LSST will be twice as good as for SDSS. Furthermore, there are close to 1000 galaxies per sensor with $r < 22$, which will provide exquisite control of systematic astrometric errors as a function of magnitude, color and other parameters, and thus enable absolute proper motion measurements.

The astrometric transformations for a given CCD and exposure, and proper motion and parallax for all the stars from a given CCD, are simultaneously solved for using an iterative algorithm. The astrometric transformations from pixel to sky coordinates are modeled using low-order polynomials and standard techniques developed at the U.S. Naval Observatory (Monet et al. 2003). The expected proper motion and parallax errors for a 10-year long baseline survey, as a function of apparent magnitude, are summarized in Table 3. Blue stars (e.g., F/G stars) fainter than $r \sim 23$ will have about 50% larger proper motion and parallax errors than given in the table due to decreased numbers of z and y band detections. The impact on red stars is smaller due to a relatively small number of observations in the u and g bands, but extremely red objects, such as L and T dwarfs, will definitely have larger errors, depending on details of their spectral energy distribution. After the first three years of the survey, *the proper motion errors are about five times as large, and parallax errors are about twice as large as the values given in Table 3; the errors scale as $t^{-3/2}$ and $t^{-1/2}$, respectively. This error behavior is a strong in-*

TABLE 3
THE EXPECTED PROPER MOTION, PARALLAX AND ACCURACY FOR A 10-YEAR LONG BASELINE SURVEY.

r mag	σ_{xy}^a mas	σ_{π}^b mas	σ_{μ}^c mas/yr	σ_1^d mag	σ_C^e mag
21	11	0.6	0.2	0.01	0.005
22	15	0.8	0.3	0.02	0.005
23	31	1.3	0.5	0.04	0.006
24	74	2.9	1.0	0.10	0.009

^a Typical astrometric accuracy (rms per coordinate per visit);

^b Parallax accuracy for 10-year long survey;

^c Proper motion accuracy for 10-year long survey;

^d Photometric error for a single visit (two 15-second exposures);

^e Photometric error for coadded observations (see Table 1).

dependent argument for a survey lifetime of at least 10 years (c.f. §2).

For comparison with Table 3, the SDSS-POSS proper motion measurements have an accuracy of ~ 5 mas/yr per coordinate at $r = 20$ (Munn et al. 2004). Gaia is expected to deliver parallax errors of 0.3 mas and proper motion errors of 0.2 mas/yr at its faint end at $r \sim 20$. Hence, LSST will smoothly extend Gaia's error vs. magnitude curve 4 magnitudes fainter.

3.4. Data Products

3.4.1. Standard processing and data products

The LSST data system is being designed to enable as wide a range of science as possible. Standard data products, including calibrated images and catalogs of detected objects and their attributes, will be provided both for individual exposures and the deep incremental data coaddition. About 2 billion objects will be routinely monitored for photometric and astrometric changes, and any transient events (non-recurrent objects with statistically significant photometric change; about 10,000 per night on average) will be posted in less than 60 seconds (with a goal of 30 seconds) via web portals including the Virtual Observatory. For the "static" sky, there will be yearly database releases listing many attributes for billions of objects. This database will grow in size to about 30 PB and about 20 billion objects⁴⁸ in ten years, and will include other metadata (parameter error estimates, system data, seeing summary, etc). For a comparison, the SDSS Data Release 6 includes about 287 million unique objects (Adelman-McCarthy et al. 2006).

The SDSS experience is that the distribution of sizes of data portal requests follows a power law, ranging from frequent simple queries or image cutout downloads to infrequent major downloads or large calculations. The same distribution is expected for LSST, and we are designing the system to enable this entire distribution. This data archive server will involve different resources deployed in different ways. We plan to optimize the mix by shipping algorithms to the data for those cases that need it (and offering local parallel computation) and transferring the data to the user for other use cases. While the data archive will be at the National Center for Supercomputing Applications (University of Illinois), we plan

⁴⁸ It is assumed that about 10 billion stars and 10 billion galaxies will be detected by LSST. The estimate of about 10 billion detected stars is sensitive to assumptions about the distribution of the interstellar dust in the Galactic plane, and cadence details. Plausible estimates range from 5 billion to 20 billion stars.

multiple data portals for community access to both the pixel data and the database. We are designing for a wide range of queries and access patterns in order to serve the broadest range of scientists as well as interested amateurs. The LSST database will be interoperable with those of surveys in other wavebands, via the Virtual Observatory.

3.4.2. Non-standard data processing and data access

The database is designed to allow evolution in the nature of the science questions that are asked of it. This design is more than simply configuring it to allow for expected growth in query complexity with time. For example, we anticipate that some users will submit queries on the images themselves. We plan for two pathways, outside of the database query system, for non-standard pixel processing. The first is through a pipeline interface that would allow a user group to attach their own pipeline processing system at a Data Access Center. This approach is appropriate for major undertakings such as an independent weak lensing analysis starting at the image level, or new ways to coadd the data. The second approach is simply to include the desired processing, such as a new quantity to be included in the Object database, within the data release processing, and pick it up on the next data release run. Much of the science will be statistical in nature and will involve large correlation calculations with user-specified precision. We plan on enabling open source community driven applications development. Finally, special data pipelines developed by the Science Collaborations (see § 5) will populate new parameters in the database.

4. EXAMPLES OF LSST SCIENCE PROJECTS

The design and optimization of the LSST system leverages its unique capability to scan a large sky area to a faint flux limit in a short amount of time. The main product of the LSST system will be a multi-color *ugrizy* image of about half the sky to unprecedented depth ($r \sim 27.5$). For a comparison, the best analogous contemporary dataset is that of SDSS, which provides *ugriz* images of about a quarter of the sky to $r \sim 22.5$, with twice as large seeing (see Figs. 20 and 21). A major advantage of LSST is the fact that this deep sky map will be produced by taking hundreds of shorter exposures (see Table 1). Each sky position within the main survey area will be observed about 1000 times, with time scales spanning seven orders of magnitude (from 30 sec to 10 years), and produce over a *trillion photometric measures* of celestial sources.

It is not possible to predict all the science that LSST data will enable. We now briefly discuss a few projects to give a flavor of anticipated studies, and organize them by the four science themes that drive the LSST design (although some projects span more than one theme).

4.1. Probing Dark Energy and Dark Matter

A unique aspect of LSST as a probe of dark energy and matter is the use of multiple cross-checking probes that reach unprecedented precision (see Fig. 22). The joint analysis of LSST weak lensing and BAO is particularly powerful in constraining the dynamical behavior

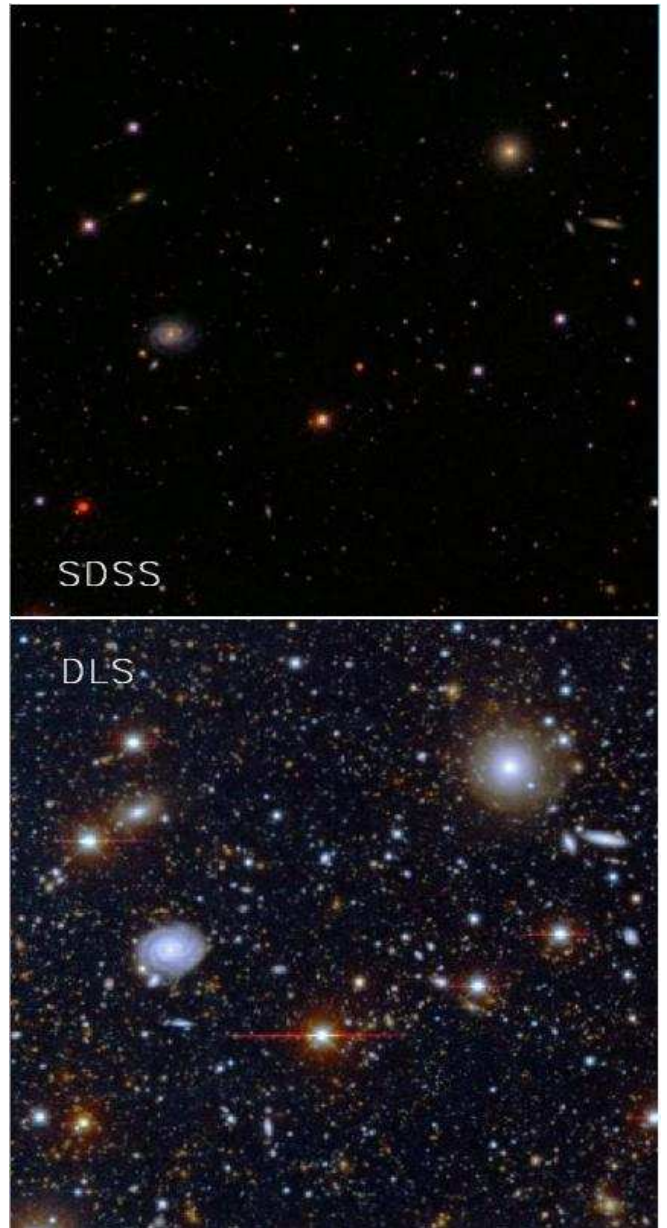


FIG. 20.— A comparison of $\sim 7.5 \times 7.5$ arcmin² images of the same area of sky (centered on $\alpha=9^h 20' 47''$ and $\delta=30^\circ 8' 12''$) obtained by the SDSS (top, $r < 22.5$) and the Deep Lens Survey (bottom, $r < 24.5$). The depth gain for the bottom image is mostly due to the lower surface brightness limit, which is also responsible for the apparent increase of galaxy sizes. LSST will obtain ~ 100 *gri* color images (~ 200 for the *riz* composites) of each point over half the Celestial sphere ($20,000 \text{ deg}^2$, equivalent to 1.3 million $\sim 7.5 \times 7.5$ arcmin² regions), and with better seeing. After their coaddition, the final image will be another ~ 3 mag deeper (a faint limit of $r = 27.5$ for point sources).

of dark energy, i.e., how it evolves with cosmic time or redshift (Hu & Jain 2004; Zhan 2006). By simultaneously measuring the growth of large-scale structure, and luminosity and angular distances as functions of redshift (via weak lensing, BAO, SN, and cluster counting), LSST data will reveal whether the recent cosmic acceleration is due to dark energy or modified gravity (Lue, Scoccimarro & Starkman 2004; Knox, Song & Tyson 2006;

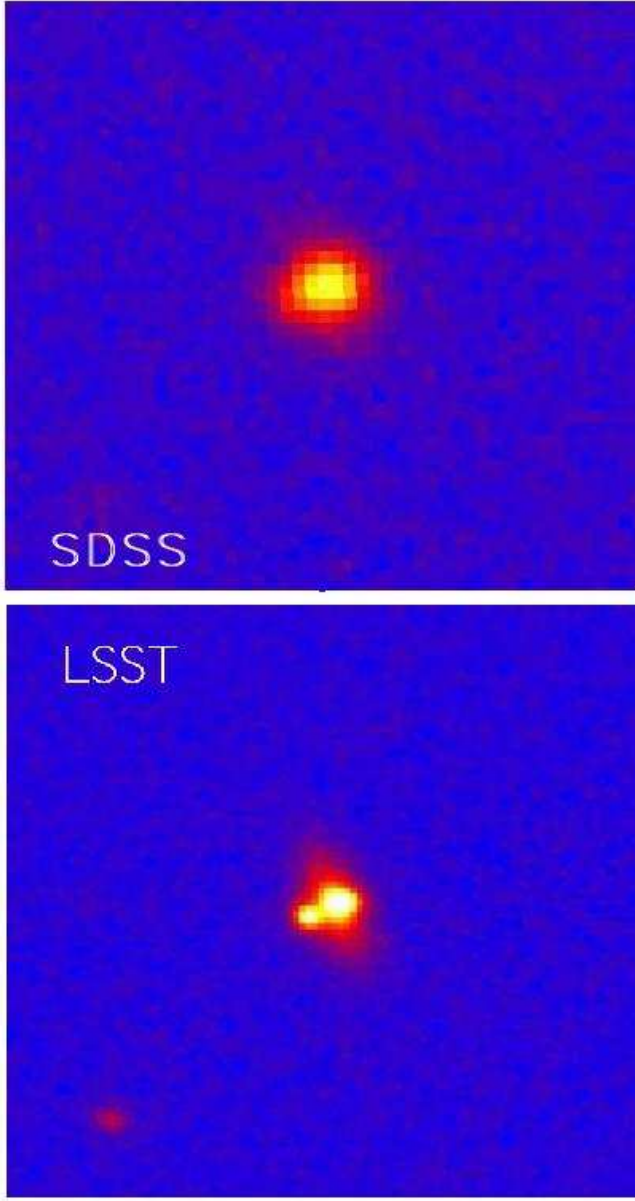


FIG. 21.— A comparison of angular resolution for images obtained by the SDSS (top, median seeing of 1.5 arcsec) and expected from LSST (bottom, seeing of 0.7 arcsec). The images show a lensed SDSS quasar (SDSS J1332+0347, Morokuma et al. 2007), and the bottom image was taken with Suprime-cam at Subaru. Adapted from Blandford et al. (2007).

Ishak, Upadhye & Spergel 2006; Jain & Zhang 2007). Over a broad range of accessible redshifts, the simple linear model for the dark energy equation of state is a poor representation of more general dark energy theories. Albrecht and Bernstein (2007) and Barnard et al. (2008) have recently shown that in a high-dimensional dark energy model space, LSST data could lead to a hundred-to thousand-fold increase in precision over precursor experiments about to be undertaken, thereby confirming its status as a premier Stage IV experiment⁴⁹.

The power and accuracy of LSST dark energy and dark matter probes is derived from samples of several billion galaxies and millions of Type Ia supernovae. The

⁴⁹ See the Dark Energy Task Force report (Albrecht et al. 2006) for a definition of Stage IV experiments.

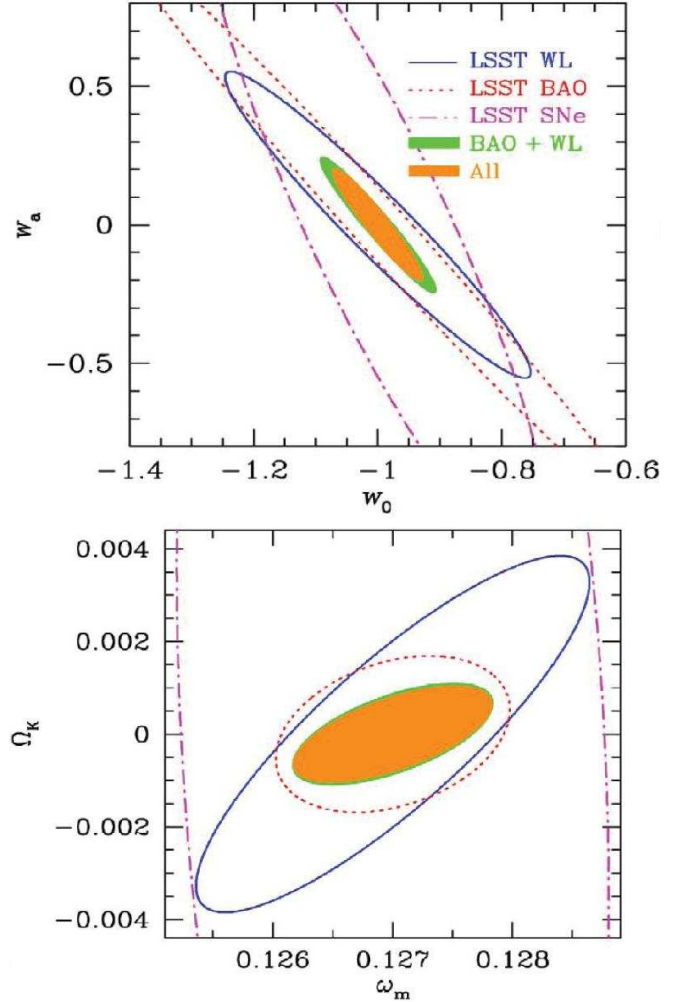


FIG. 22.— The top panel shows forecasts of LSST errors on the dark energy equation-of-state parameters w_0 and w_a ($w(z) = P/\rho = w_0 + (1 - a)w_a$, where $a = (1 + z)^{-1}$) for measurements based on baryon acoustic oscillations, weak lensing, supernovae and the three combined. The constraints are marginalized over 9 other cosmological parameters including the curvature and over 120 parameters that model the linear galaxy clustering bias, photometric redshift bias, and rms photometric redshift error (Zhan 2006). Simple additive systematic errors of the shear and galaxy power spectra are also included. The joint analysis of BAO and WL significantly reduces the error ellipse area because the error distribution of photometric redshifts can be calibrated with galaxy power spectra, and the galaxy bias can be determined with galaxy and WL shear power spectra. The bottom panel is analogous to the top panel, but for the physical matter density $\omega_m = \Omega_m h^2$ and curvature term Ω_k . Combining all of LSST's cosmological probes further increases the precision. Different theoretical models of dark energy span this w_0 - w_a space.

nominal high-SNR sample defined by $i < 25$ (SNR > 25 for point sources) will include four billion galaxies (56 arcmin⁻²) with a mean photometric redshift accuracy of 1-2% (relative error for $1 + z$), and with only 10% of the sample with errors larger than 4%. The median redshift for this sample will be $z \sim 1.2$, with the third quartile at $z \sim 2$. For a subsample of 2 billion galaxies further constrained by flux limits in the g and z bands, the photometric redshift errors will be two to three times smaller. It may be possible to further improve photometric redshift calibration using non-conventional methods (Newman 2008). The surface density of galaxies useful for weak lensing analysis will be about 40 arcmin⁻².

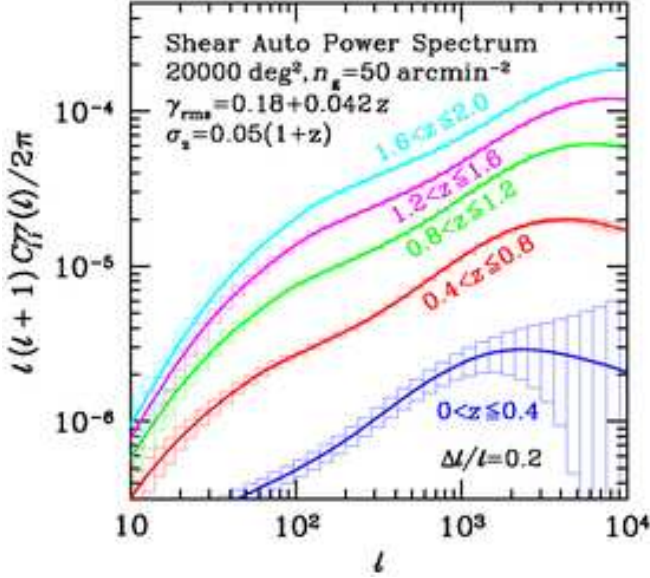


FIG. 23.— The lensing shear auto power spectra constructed from 5 redshift bins (ℓ is the multipole moment of the distribution on the sky). Only the 5 auto-power spectra of each redshift bin among the available 15 cospectra are displayed, and the solid curves show the predictions for the concordance Λ CDM model. The boxes show the expected $1-\sigma$ measurement error ($\Delta\ell/\ell = 0.2$) from the full LSST 10-year survey due to the sample (i.e., cosmic) variance which dominates at about $\ell < 1000$, and intrinsic ellipticities which dominate at $\ell > 1000$ (Zhan 2006).

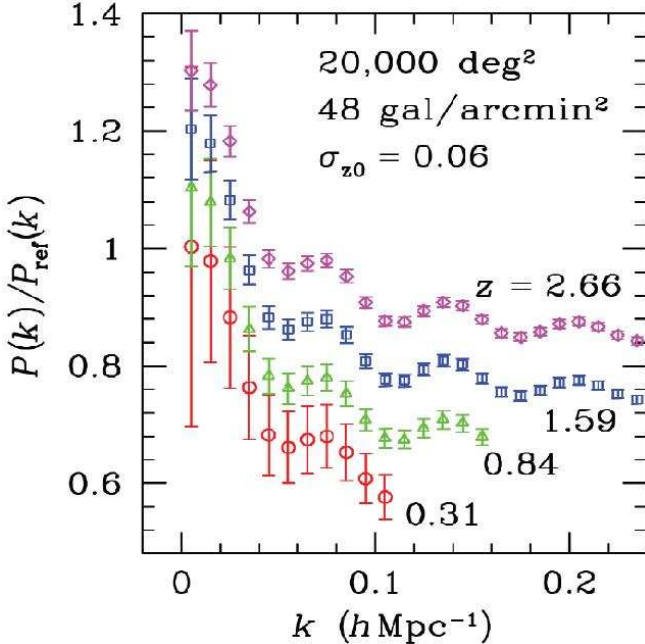


FIG. 24.— Simulations of the ratio of the measured galaxy power spectrum to a featureless reference power spectrum in various redshift bins (shifted vertically for clarity), for the full LSST survey using very conservative photometric redshift errors. The several peaks visible in each curve are the signature of baryon acoustic oscillations (Eisenstein et al. 2005; Cole et al. 2005). LSST will measure the angular diameter distance over this redshift range with an accuracy of $\sim 1\%$ (Zhan & Knox 2006).

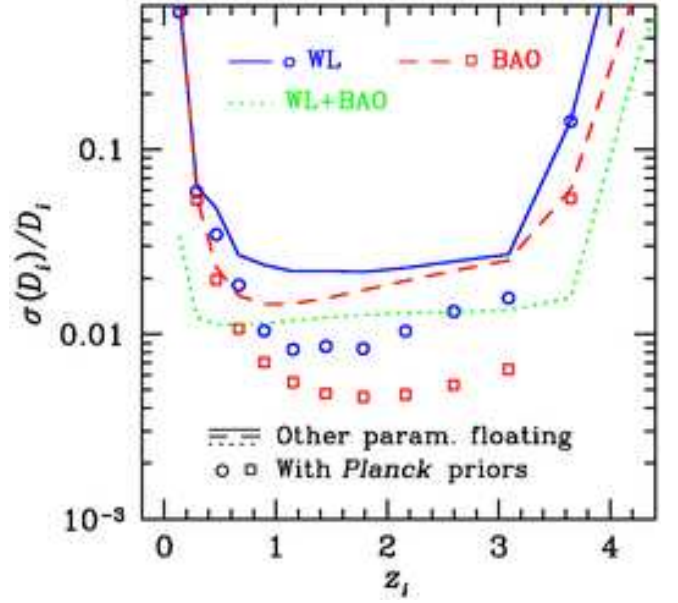


FIG. 25.— Marginalized $1-\sigma$ errors on the comoving distances from LSST WL (solid line and open circles), BAO (dashed line and open squares), and joint WL and BAO (dotted line). The distance parameters, $D_1 \dots D_{14}$, are evenly spaced in $\log(1+z)$ from $z_1=0.14$ to $z_{14}=5$. Lines represent results with cosmological parameters floating, i.e., marginalized with weaker-than-5-year-WMAP priors, and symbols are for results with Planck priors (Zhan, Knox & Tyson 2008, in prep).

The main LSST deliverables in the context of dark energy and matter will be

- Multiple cosmic 2-point shear probes (Fig. 23). There will be over 50 of these auto and cross power spectra constructed using 3-D shear tomography (correlation of shear of a galaxy at one redshift bin with another galaxy in a different redshift bin, averaged over all pairs of billions of galaxies; Jain & Taylor 2003).
- Higher-order shear and galaxy statistics that can improve dark energy constraints and provide self-calibration of various systematics (Takada & Jain 2004; Dolney, Jain & Takada 2006; Huterer et al 2006). They are also probes of both primordial non-Gaussianities and those caused by non-linear structure.
- Baryon Acoustic Oscillations in the galaxy angular correlation functions. The standard ruler of the sound horizon at decoupling which is imprinted on the mass distribution at all redshifts provides a direct way of measuring the angular diameter distance as a function of redshift (Fig. 24; Eisenstein, Hu & Tegmark 1998; Cooray et al. 2001; Blake & Glazebrook 2003; Hu & Haiman 2003; Linder 2003; Seo & Eisenstein 2003). LSST photo- z BAO will achieve percent level precision on the angular diameter distance at ~ 10 redshifts logarithmically spaced between $z = 0.4$ to 3.6 with this CMB-calibrated standard ruler (Fig. 25). When combined with CMB and weak lensing (WL) cosmic shear, this probe yields tight constraints on the dynamical behavior of dark energy. In particular, high-redshift BAO data can break the degeneracy

between curvature and dark energy, and constrain Ω_k to within 0.001, which is ten times better than the most accurate current result based on WMAP and SDSS data (Tegmark et al. 2006; Spergel et al. 2007).

- Supernovae. The two LSST samples are complementary: the main survey will obtain light curves in 6 bands and photometric redshifts of about million Type Ia supernovae per year (permitting a search for a “third parameter” which, if not understood, might introduce systematic error in luminosity evolution; Wood-Vasey et al. 2007), and the rapid sampling “mini-survey” of selected areas will yield well sampled light curves of tens of thousands of supernovae to a limiting redshift beyond one (leading to an independent test of dark energy dynamics; Riess et al. 2007).
- The distribution of strongest WL shear peaks with redshift. This is a simultaneous probe of the universal mass function and the growth of structure, and provides an important constraint on dark energy (Wang et al. 2005). LSST will find over 200,000 such shear peaks on galaxy cluster scales.
- Unique constraints on anisotropy of cosmological parameters over the sky using SN, lensing clusters and lensing galaxies, which will test fundamental cosmological assumptions of homogeneity and isotropy.
- The shape of the power spectrum of dark matter fluctuations measured by the LSST weak lensing maps will constrain the sum of neutrino masses with an accuracy of 0.04 eV or better (Cooray 1999; Song & Knox 2004; Hannestad, Tu & Wong 2006). The current best limit, as derived from a combination of WMAP, the SDSS power spectrum, SN, and the Ly α forest, is 0.17 eV (Seljak et al. 2006).
- Several millions of galaxy-galaxy lenses will provide the needed statistics to constrain the dark matter mass function on small scales, and to probe dark matter halo profiles and substructure (Mandelbaum et al. 2006).
- LSST will discover several hundred strong lensing clusters in which background objects are multiply lensed. Cluster mass reconstruction based on the multiple image data and time delays between them (from SN or AGN activity) can probe the cluster inner mass profile, and can provide a separate test of cosmology, especially in cases with strongly lensed background objects at different redshift (Porciani & Madau 2000; Oguri & Kawano 2003).
- Time delays for QSOs multiply lensed by clusters as a function of redshift are an independent test of dark energy (Kundić et al. 1997). The natural timescale (many months to years) is well matched to the LSST survey.

4.2. Taking an Inventory of the Solar System

The small bodies of the Solar System, such as main-belt asteroids, the Trojan populations of the giant planets and the Kuiper Belt objects, offer a unique insight into its early stages because they provide samples of the original solid materials of the solar nebula. Understanding these populations, both physically and in their number and size distribution, is a key element in testing various theories of the Solar System formation and the evolution.

The baseline LSST cadence will result in orbital parameters for several million moving objects; these will be dominated by main-belt asteroids, with light curves and multi-color photometry for a substantial fraction of detected objects. This dataset will yield 10 to 100 times more objects than are currently available with orbits, colors, and variability information. As already discussed in detail (§ 3.3.2), LSST is capable of reaching the Congressional target completeness of 90% for PHAs larger than 140 m, and will detect over 30,000 TNOs brighter than $r \sim 24.5$ using its baseline cadence. LSST will be capable of detecting objects like Sedna to beyond 100 AU, thus enabling *in situ* exploration far beyond the edge of the Kuiper belt at ~ 50 AU. Because most of these objects will be observed several hundred times, accurate orbital elements, colors, and variability information will also be available.

Among the Solar System studies, these data will enable:

- Studies of the distribution of orbital elements for several million main-belt asteroids as a function of color-based taxonomy (see Fig. 26) and size; size distributions of asteroid families (Parker et al. 2008) and their correlations with age (Jedicke et al. 2004; Nesvorný et al. 2005); dynamical effects (Bottke et al. 2001); and studies of object shapes and structure using light curves (Pravec & Harris 2000).
- Studies of the distribution of orbital elements for about 100,000 NEOs as a function of color and size (Rabinowitz 1993; Dandy, Fitzsimmons & Collander-Brown 2002). Correlations with the analogous distributions for main-belt objects, and studies of object shapes and structure using light curves.
- Studies of the distribution of orbital elements for about 100,000 Jovian Trojan asteroids as a function of color and size (Jewitt, Trujillo & Luu 2000; Yoshida & Nakamura 2005; Szabo et al. 2007); the search for dynamical families (Knežević & Milani 2005); studies of shapes and structure using light curves.
- Studies of the distribution of orbital elements for over 30,000 TNOs (see Fig. 27) as a function of color and size; the search for dynamical families; studies of shapes and structure using light curves (Duncan & Levison 1995; Trujillo, Jewitt & Luu 2001; Gladman et al. 2001; Bernstein et al. 2004; Elliot et al. 2005; Jones et al. 2006; Doressoundiram et al. 2007).

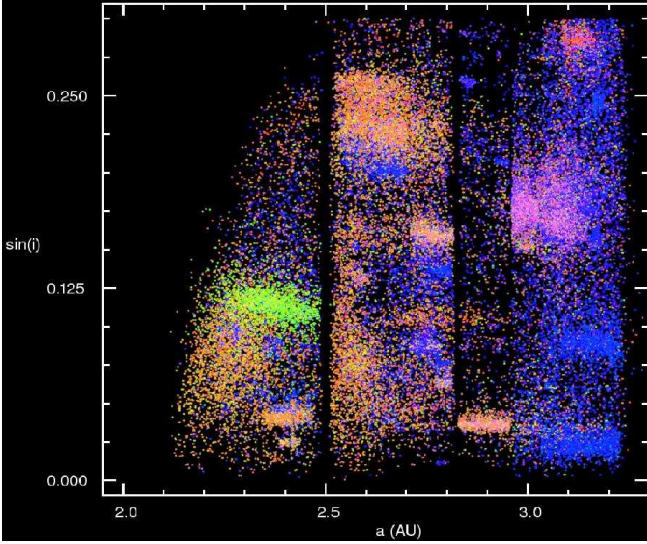


FIG. 26.— An example of color-based asteroid taxonomy. The figure shows the distribution of asteroids in the proper semi-major axis vs. $\sin(i)$ plane for 45,000 asteroids with colors measured by SDSS (Parker et al. 2008). The color of each dot is representative of the object's color. Note the strong correlation between asteroid families (objects in distinct regions of the plane) and colors. There are at least five different taxonomic types distinguishable with SDSS measurements, and LSST color measurements of asteroids will be more than twice as accurate (and will increase the number of objects by ~ 2 orders of magnitude).

- An unbiased and complete census of both Jupiter-family and Oort-cloud comets; 6-band sub-arcsecond spatial profiles to a faint surface brightness limit; temporally resolved activity (Lowry et al. 1999; A'Hearn 2004).
- The search for objects with perihelia at several hundred AU. For example, an object like Sedna (Brown, Trujillo & Rabinowitz 2004) will be detectable at 130 AU.
- Studies of the solar wind propagation speed using induced activity in a large sample of comets at different heliocentric distances (B. Vršnak, priv. comm.)

4.3. Exploring the Transient Optical Sky

Time domain science will greatly benefit from LSST's unique capability to simultaneously provide large area coverage, dense temporal coverage, accurate color information, good image quality, and rapid data reduction and classification. Since LSST extends time-volume space a thousand times over current surveys (e.g., Morokuma et al. 2008), the most interesting science may well be the discovery of new classes of objects. There are many projects that LSST data products will enable:

- Detection and measurement of gamma-ray burst afterglows and transients (e.g., Zhang & Mészáros 2004) to high redshift (~ 7.5).
- Studies of optical bursters (those varying faster than 1 mag/hr) to $r \sim 25$ mag.
- Gravitational micro-lensing in the Local Group and beyond (de Jong, Kuijken & Héraudeau 2008).

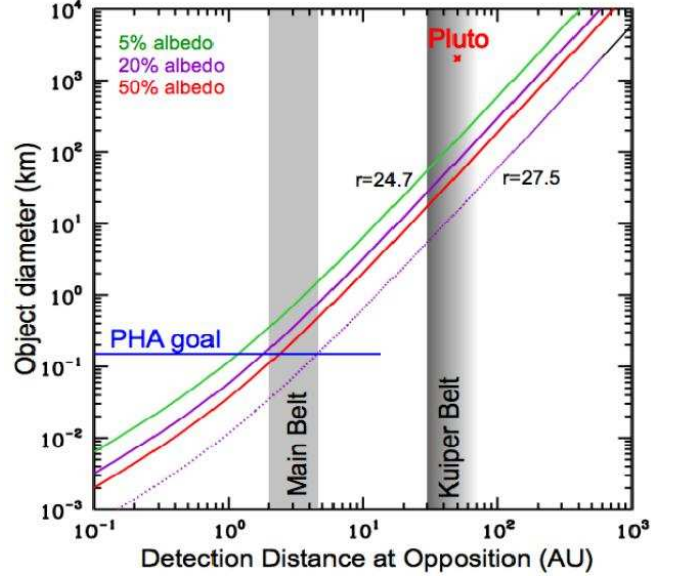


FIG. 27.— The LSST detection limits for distant solar system objects. Moving objects with diameters as small as 100m in the main asteroid belt and 100km in the Kuiper Belt (TNOs) will be detected. Specialized deeper observations (see § 3.2.2) will detect TNOs as small as 10 km. Adapted from Jones et al. (2007).

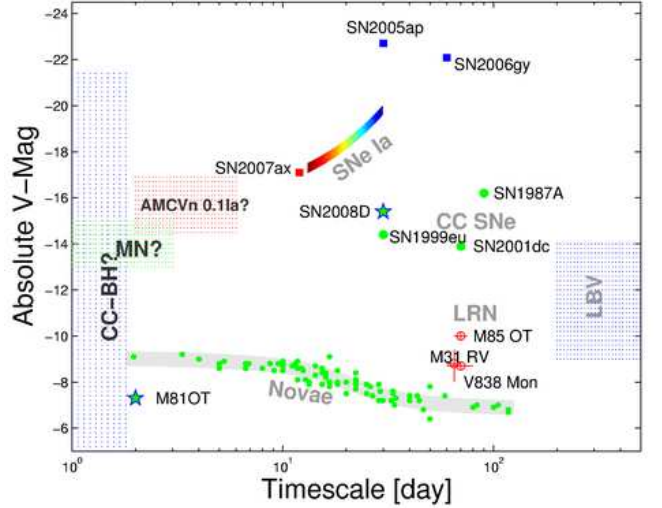


FIG. 28.— The phase space of cosmic explosive and eruptive transients as represented by their absolute V band peak brightness (y axis) and the event timescale (adapted from Kulkarni et al. 2006). LSST will open up large regions of this phase space for systematic exploration by extending time-volume space 1000 times over existing surveys.

- Studies of SN populations and parametrization of light curves (e.g., Hoefflich, Wheeler & Thielemann 1998; Howell et al. 2007).
- Studies of dwarf novae, including their use as probes of stellar populations and structure in the Local Group (Neill & Shara 2005).
- A deep search for new populations of novae and supernova progenitors (Kulkarni et al. 2006; see Fig.28).
- Search for stellar tidal disruptions by nuclear supermassive black holes (Evans & Kochanek 1989; Gezari et al. 2008).

- A study of quasar variability using 1-2% accurate, multicolor light curves for ~ 2 million quasars, leading to constraints on the accretion physics (de Vries, Becker & White 2003; Vanden Berk et al. 2004).
- Optical identifications for transients detected at other wavelengths, from gamma-rays to radio, as well as by means other than electro-magnetic radiation (e.g., LIGO⁵⁰, LISA⁵¹, ICECUBE⁵²)
- The superb continuum light curves of AGN will enable economical "piggyback" reverberation-mapping efforts using emission lines (Liu et al. 2008). These results will greatly broaden the luminosity-redshift plane of reverberation-mapped AGNs with black-hole mass estimates. For LSST data alone, the inter-band continuum lags will provide useful structural information.
- LSST data will allow good constraints on AGN lifetimes due to large sample size and survey lifetime (e.g., Martini & Schneider 2003).

4.4. Mapping the Milky Way

The LSST will map the Galaxy in unprecedented detail, and by doing so revolutionize the fields of Galactic Astronomy and Near-field Cosmology. The great detail with which the Milky Way can be studied complements the statistical power of extra-galactic observations. The overarching goal of near-field cosmology is to use spatial, kinematic, and chemical data sets of stars to reveal the structure and evolution history of the Milky Way and its environment. LSST will reveal this fossil record in great detail and provide a Rosetta Stone for extragalactic astronomy by setting the context within which we interpret these broader data sets. Moreover, by providing a census of faint satellites and stellar streams in the halo, this map will offer a unique means to constrain the particle nature of dark matter because candidate supersymmetric particle dark matter models predict different mass clustering on small scales, with a corresponding range of mass profiles in low-mass systems.

The LSST will produce a massive and exquisitely accurate photometric and astrometric data set for about 10 billion Milky Way stars. The coverage of the Galactic plane will yield data for numerous star-forming regions, and the y band data will penetrate through the interstellar dust layer. Photometric metallicity measurements (see Figs. 29 and 30) will be available for about 200 million main-sequence F/G stars which will sample the halo to distances of 100 kpc (Ivezić et al. 2008). No other existing or planned survey will provide such a massive and powerful dataset to study the outer halo, including Gaia which is flux limited at $r = 20$, the SkyMapper which is flux limited to $r = 22.6$ (but will nicely complement SDSS in the Southern hemisphere), and Pan-STARRS which will not have the u band (which is necessary for estimating metallicity). The LSST in its standard surveying mode will be able to detect RR Lyrae variables

(pulsating stars and standard candles) and classical novae (exploding stars and standard candles) at a distance of 400 kpc and hence explore the extent and structure of our own halo out to half the distance to the Andromeda galaxy. Thus, the LSST will enable studies of the distribution of main-sequence stars beyond the presumed edge of the Galaxy's halo (see Fig. 31), of their metallicity distribution throughout most of the halo, and of their kinematics beyond the thick disk/halo boundary. It will also obtain direct distance measurements via trigonometric parallax below the hydrogen-burning limit for a representative thin-disk sample.

In addition to the study of hydrogen burning stars, LSST will uncover the largest sample of stellar remnants to date. Over 97% of all stars eventually exhaust their fuel and cool to become white dwarfs. Given the age of the Galactic halo, most of the mass in this component is now tied up in these remnant stars (e.g., Alcock et al. 2000) and therefore their discovery directly constrains the Galactic mass budget. These large populations of disk and halo white dwarfs will provide unprecedented constraints on the luminosity function of these stars, which will directly yield independent ages for the Galactic disk and halo (e.g., through the initial-final mass relation, Kalirai et al. 2008).

The spatial coverage of LSST naturally targets both field stars and star clusters. To date, no systematic survey of the stellar populations of Southern hemisphere clusters has been carried out (e.g., such as the CFHT Open Star Cluster Survey or the WIYN Open Star Cluster Survey in the North; Kalirai et al. 2001; Mathieu 2000). Multiband imaging of these co-eval, co-spatial, and iso-metallic systems will provide vital insights into fundamental stellar evolution. For example, the depth of LSST will enable us to construct luminosity and mass functions for nearby open clusters down to the hydrogen burning limit. Variations in the initial mass function will be studied as a function of environment (e.g., age and metallicity). The wide-field coverage will also allow us to track how the stellar populations in each cluster vary as a function of radius, from the core to beyond the tidal radius. Fainter remnant white dwarfs will be uncovered in both open and globular clusters (the nearest of which are all in the South) thereby providing a crucial link to the properties of the now evolved stars in each system.

In summary, the LSST data will revolutionize studies of the Milky Way and the entire Local Group (Saha et al. 2007). We list a few specific Galactic science programs that LSST will enable:

- High-resolution studies of the distribution of stars in the outer halo in the six-dimensional space spanned by position, metallicity and proper motions (e.g., Girard et al. 2006; Bell et al. 2007; Jurić et al. 2008).
- The faintest ever search for halo streams, and galaxy satellites and intergalactic stars over much of the Local Group (e.g., Grillmair 2006ab; Ibata et al. 2007; Walsh, Jerjen & Willman 2007; Belokurov et al. 2007a).
- Deep and highly accurate color-magnitude diagrams for over half of the known globular clusters, including tangential velocities from proper motion

⁵⁰ <http://www.ligo.caltech.edu>

⁵¹ <http://lisa.nasa.gov>

⁵² <http://icecube.wisc.edu>

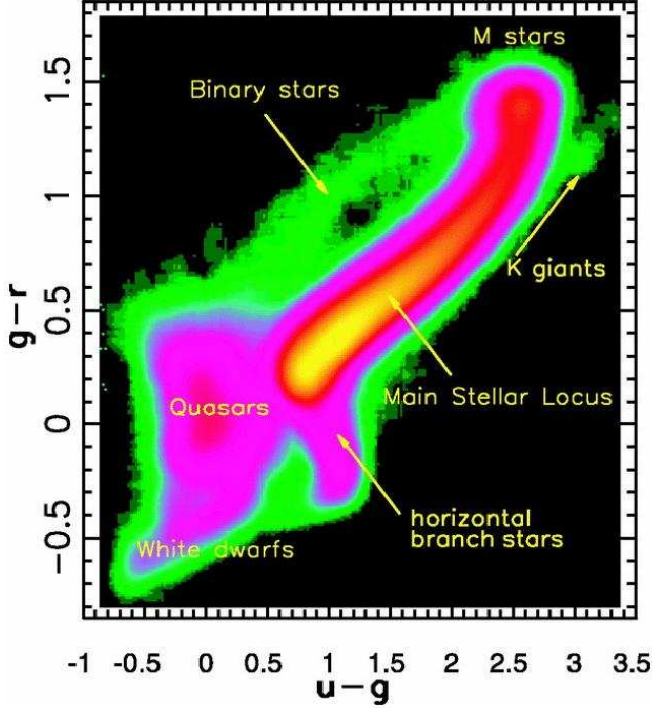


FIG. 29.— The $g-r$ vs. $u-g$ color-color diagram for two million stars measured by SDSS (adapted from Smolčić et al. 2004). Accurate multi-color photometry contains information that can be used for source classification and determination of detailed stellar properties such as effective temperature and metallicity. LSST will enable such measurements for billions of stars.

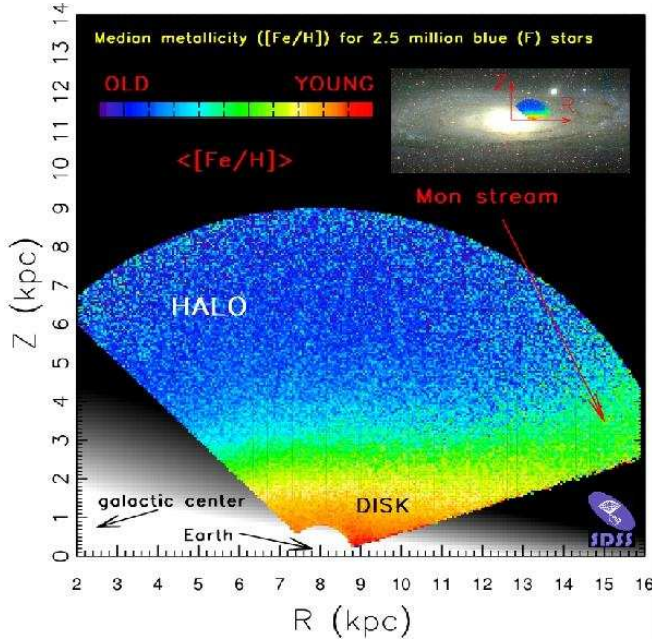


FIG. 30.— The median metallicity map for 2.5 million main-sequence F-type stars within 10 kpc from the Sun (adapted from Ivezić et al. 2008). The metallicity is estimated using $u-g$ and $g-r$ colors measured by SDSS. The position and size of the mapped region, relative to the rest of the Milky Way, is illustrated in the top right corner, where the same map is scaled and overlaid on an image of the Andromeda galaxy. The gradient of the median metallicity is essentially parallel to the Z axis, except in the Monoceros stream region, as marked. LSST will extend this map out to 100 kpc, using a sample of over 100 million main-sequence F stars.

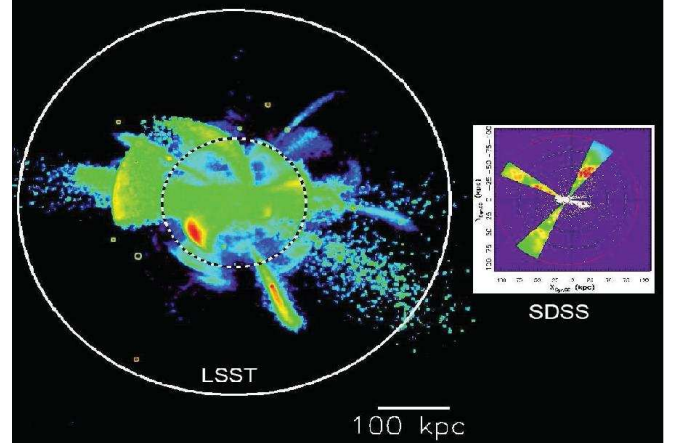


FIG. 31.— A simulation of the outer regions of the Milky Way (left), compared to the current state-of-the-art data (right), shown on the same spatial scale. The data panel shows the number density multiplied by the cube of the Galactocentric radius (logarithmic scale with dynamic range of 1000, from blue to red), for ~ 1000 SDSS RR Lyrae stars within 10 degrees of the Sgr dwarf tidal stream plane (Ivezić et al. 2003). The same color coding was used to visualize stellar number density for a Milky Way type galaxy simulation from Bullock and Johnston (2005), shown on the left. Set with an Λ CDM merger history, these simulations track the accretion and disruption of hundreds of dwarf galaxies into Milky-Way size halos. With LSST, RR Lyrae stars will be found beyond the presumed Milky Way tidal radius (~ 300 kpc, white circle), and much more numerous main-sequence stars will trace the structure out to 100 kpc (dashed circle), with similar fidelity as shown in Figure 30. The latter distance range can now be probed only using RR Lyrae stars and other rare non-main-sequence stars.

measurements (Casetti-Dinescu et al. 2007; Clem, VandenBerg & Stetson 2008).

- Mapping the metallicity, kinematics and spatial profile of the Sgr dwarf tidal stream (e.g., Ibata et al. 2001; Majewski et al. 2003; Law, Johnston & Majewski 2005).
- Studies of the clumpiness of the gravitational potential in the Galaxy using fragile wide-angle binaries selected with the aid of trigonometric and photometric parallaxes, and common proper motion (e.g., Yoo, Chanamé & Gould 2004).
- Detailed studies of variable star populations; 2% or better accurate multicolor light curves will be available for a sample of at least 50 million variable stars (Sesar et al. 2007), enabling studies of cataclysmic variables, eclipsing binary systems, rare types of variables, etc.
- Discovery of rare and faint high proper motion objects: probing the faint end of the stellar mass function (Lepine 2008), and searching for free-floating planet candidates (Lucas & Roche 2000).
- Direct measurement of the faint end of the stellar luminosity function using trigonometric parallaxes (Gratton et al. 1997). A complete census of the solar neighborhood to a distance of 100 pc based on trigonometric parallax measurements for objects as faint as $M_r = 17$. For example, LSST will deliver 10% or better distances for a sample of about 2,500 stars with $18 < M_r < 19$. There are only a handful of such stars known today (and Gaia will detect fewer than 100).

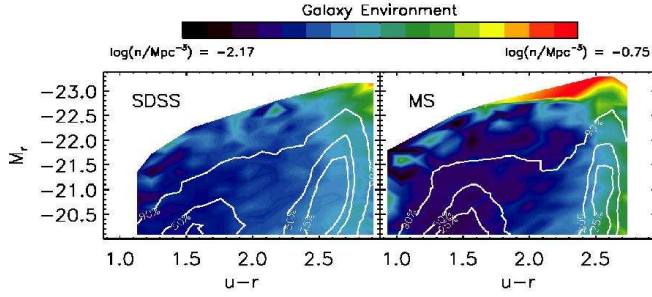


FIG. 32.— A comparison of the distribution of galaxies in luminosity-color-density space measured by SDSS (left) and a model based on the Millennium simulation (right). The linearly-spaced contours outline the distribution of volume-limited sample of galaxies in the plotted diagram, and the color-coded background shows the median environmental density (computed using the ten nearest neighbors) for galaxies with the corresponding luminosity and color. Such multi-variate distributions encode rich information about formation and evolution of galaxies. Galaxies detected by SDSS are representative of the low-redshift Universe (the median redshift is ~ 0.1). The LSST will enable such studies as a function of redshift, to $z \sim 2$. Adapted from Cowan & Ivezić (2008).

- Using their rich molecular band structure, the LSST colors (especially the $z - y$ color) and faint limit will permit the separation of halo M subdwarfs from disk M dwarfs (West et al. 2004; Lepine & Scholz 2008).
- Planetary transits: the data set may include a mini survey of 600 sq.deg. of sky which will collect about 40 hour-long sequences of 200 observations each over a 4-month period (see § 3.2.2). There would be an additional 800 observations over 10 years of these same fields as part of the main survey. With about 10 million or more stars in the sample (depending on where the fields are placed), this would provide an excellent material to study the planet frequency as a function of stellar type, metallicity, and distance from the Galactic plane (e.g., Charbonneau et al. 2000; Konacki et al. 2003).
- A complete census of AGB stars in the Galaxy by searching for resolved envelopes and optical identifications of IR counterparts (e.g., from IRAS and Spitzer surveys), and by using long-term variability and color selection (Ivezić 2007c).
- A complete census of faint populations in nearby star forming regions using color and variability selection (e.g., Briceno et al. 2005).
- High-resolution three-dimensional studies of interstellar dust using 5-color SEDs of main sequence stars (McGehee 2004; Meyer et al. 2005).

4.5. Additional Science Projects

The experience with any large survey (e.g., SDSS, 2MASS, GALEX, to name but a few) is that the most interesting science that comes out is often unrelated to the main science drivers, and is unanticipated at the time the survey is designed. LSST will enable even more diverse science than encompassed by the four themes that drive the system design. We list a few anticipated major programs.

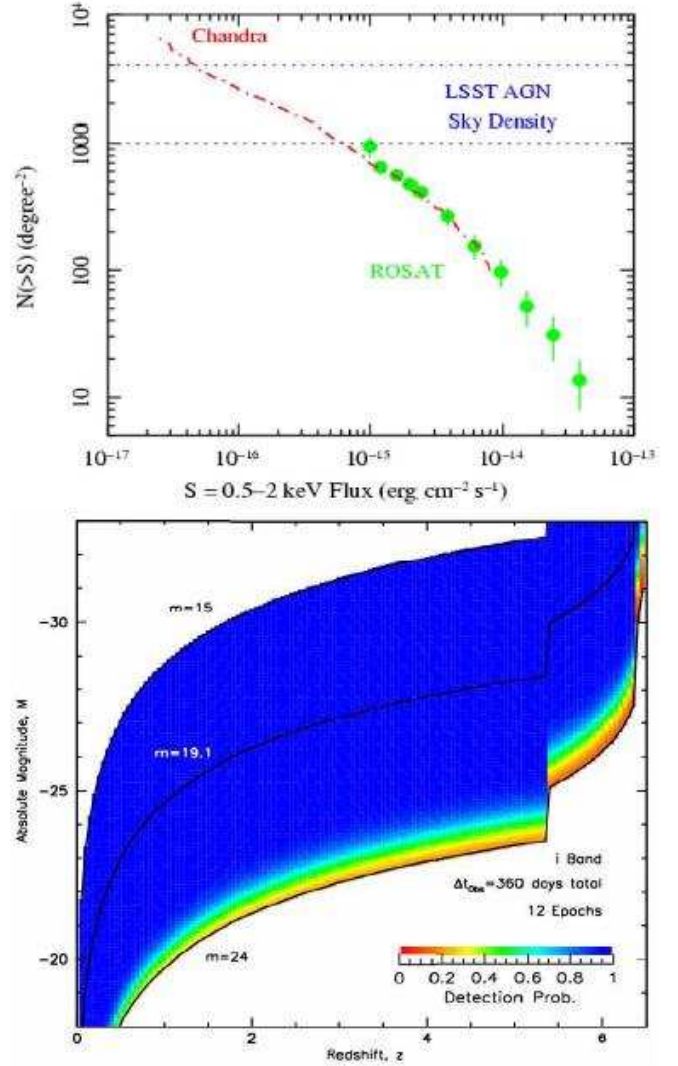


FIG. 33.— The LSST will deliver AGN sky densities of 1000-4000 deg^{-2} , which is competitive with the deepest pencil-beam surveys to date, such as the Chandra Deep Fields (top panel). The total LSST AGN yield, selected using colors and variability, should be 20-80 million objects. The bottom panel shows the expected distribution of these objects in the absolute magnitude vs. redshift plane, color-coded by the probability for an object to be detected as variable after 1 year of observations. Note that quasars will be detected to their formal luminosity cutoff ($M < -23$) even at redshifts of ~ 5 . Adapted from Brandt et al. (2007).

- Detailed studies of galaxy formation and evolution using their distribution in luminosity-color-morphology space as a function of redshift. For example, LSST will enable studies of the rest-frame UV emission, similar to those based on GALEX data for local galaxies, to a redshift of ~ 2 . These studies project onto many axes (see Fig. 32):

- the evolution of the galaxy luminosity function with redshift, as a function of morphology and color
- the evolution of the galaxy color distribution over a wide range of rest-frame wavelengths, and as a function of luminosity and morphology
- bulge-disk decomposition, as a function of luminosity and color, over a large redshift range

- detailed distribution of satellite galaxies in luminosity-color-morphology space as a function of luminosity, color, and morphology of the primary galaxy
 - correlations of luminosity, color and morphology with local environment, and as a function of redshift
 - the properties of galaxy groups as a function of cosmic time.
- AGN census to a very faint luminosity limit and to a large redshift limit, yielding 20-80 million objects (see Fig. 33). By pushing substantially further down the AGN luminosity function over a very large solid angle, LSST data will lead to a much clearer understanding of black-hole growth during the first Gyr. For example, LSST should discover ~ 1000 AGNs at $z \sim 6.5 - 7.5$ at the end of the dark ages, representing a dramatic increase over the present samples (Brandt et al. 2007).
 - The first half-sky survey of ultra low surface brightness objects, with photometric redshift information. The currently available samples are highly incomplete, especially in the Southern Hemisphere (see Fig. 7 in Belokurov et al. 2007a).
 - Search for strong gravitational lenses to a faint surface brightness limit (e.g., Bartelmann et al. 1998; Tyson, Kochanski & Dell’Antonio 1998; Belokurov et al. 2007b).
 - Multi-wavelength studies of faint optical sources using X-ray, IR and radio data. For example, SDSS detected only 1/3 of all 20cm FIRST sources (Becker et al. 1995) because it was too shallow by ~ 4 mag for a complete optical identification.

4.5.1. Synergy with other projects

LSST will not operate in isolation and will greatly benefit from other precursor and coeval data at a variety of wavelengths, depths, and timescales. For example, most of the Celestial Sphere will be covered to a limit several magnitudes fainter than LSST saturation ($r \sim 16$), first by the combination of SDSS, PS1 and SkyMapper (Keller et al. 2001), and then by the Gaia survey. The SkyMapper survey will obtain imaging data in the southern sky to similar depths as SDSS, the Pan-STARRS surveys will provide multi-epoch data deeper than SDSS in the northern sky, and the Dark Energy Survey (Flaugher 2006) will scan $\sim 5000 \text{ deg}^2$ to similar depth as Pan-STARRS in the southern sky. Despite the lack of the u band data and a shallower depth by about a magnitude, the Pan-STARRS surveys will represent a valuable complement to LSST in providing an all-sky coverage to a limit fainter than that of SDSS and SkyMapper. LSST and Gaia will be complementary datasets for studying the Milky Way in the multi-dimensional space of three-dimensional positions, proper motions and metallicity. The Gaia survey will provide calibration checks at the bright end for proper motions and trigonometric parallax measurements by LSST, and LSST will extend the Gaia survey four magnitudes deeper. The LSST data

stream will invigorate subsequent investigations by numerous other telescopes that will provide additional temporal, spectral and spatial resolution coverage.

LSST will provide a crucial complementary capability to planned space experiments operating in other bands, such as the Gamma-Ray Large Area Space Telescope (GLAST⁵³) and the Black Hole Finder Einstein Probe Mission. The Laser Interferometer Space Antenna (LISA) is designed to study black hole mergers through the gravitational wave outburst that should be emitted during the final stages of such events. LSST has the potential to measure the electromagnetic signal that accompanies the gravitational wave emission, thereby providing a definite position on the sky for the system, which is crucial for follow-up observations. LSST will also make the archives for billion-dollar class space missions such as Chandra, XMM-Newton, Spitzer, etc., much more valuable, because deep optical multi-color data will enable massive photometric follow-up studies of sources from these missions. Last but not least, the huge samples of various astronomical source populations will yield extremely rare objects for follow-up by powerful facilities such as JWST (Gardner et al. 2006) and GSMT (Kan & Antebi 2003).

In summary, the diversity of science enabled by LSST will be unparalleled, extending from the physics of gravity and the early Universe to the properties of “killer” asteroids (PHAs). While there are other projects that aim to address some of the same science goals, no other project matches this diversity and LSST’s potential impact on society in general.

5. COMMUNITY INVOLVEMENT

LSST has been conceived as a public facility: the database that it will produce, and the associated object catalogs that are generated from that database, will be made available to the scientific community and to the public at large with no proprietary period. The LSST data management system will provide user-friendly tools to access this database and to support user-initiated queries, run on LSST computers, either at the archive facility or at the data access centers. We expect that many, perhaps even the majority of LSST discoveries will come from research astronomers with no formal affiliation to the project, from students, and from interested amateurs, intrigued by the accessibility to the Universe that this facility uniquely provides. For example, because of its interest in the large public data access of the LSST program, the Google Corporation has recently joined the LSST team.

The SDSS provides a good example for how the scientific community can be effective in working with large, publicly available astronomical data sets. The SDSS has put out a series of large incremental data releases via a sophisticated database, roughly once per year, together with a paper describing the content of each data release, and extensive on-line documentation giving instructions on downloading the catalogs and image data (see <http://www.sdss.org>). Over 60% of the more than 1800 refereed papers based on SDSS data to date (May 2008) have been written by people from outside the project, and include many of the most high-profile re-

⁵³ <http://glast.gsfc.nasa.gov>

sults that have come from the facility.

Nevertheless, it is clear that many of the highest priority LSST science investigations will require organized teams of professionals working together to optimize science analyses and to assess the importance of systematic uncertainties on the derived results. To meet this need, ten science collaborations have already been established by the project in core science areas (Strauss 2007).

As of the time of this contribution, there are close to 200 participants in these collaborations, mostly from LSST member institutions. As the project proceeds into development, an open call for applications for membership will be issued to the professional community at large. It is anticipated that the LSST science collaborations will perform their analyses using LSST computational facilities, and the system has been sized accordingly.

As we design our observing strategies, we are actively seeking and implementing input by the wide community of scientists in the LSST Science Collaborations. Their task, among others, is to enhance the LSST science case and provide advice on how to optimize their science with choices in cadence, software, and data systems. The Science Collaborations are expected to play a major role in the system optimization during the commissioning period. We will continue this review when the survey starts, and will maintain our design of flexible cadence structure.

6. EDUCATIONAL AND SOCIETAL IMPACTS

The impact – and enduring societal significance – of the LSST will exceed its direct contributions to advances in physics and astronomy. With an open database available in real time to the non-specialist public, LSST has the capacity to literally bring the Universe home to everyone. The “movie of the Universe” will offer a new window on the sky for curious minds of all ages. Any interested amateur, anywhere in the world, will be able to log on to his or her computer and look at the latest images of any part of the sky⁵⁴. In the context of open source development, as we have witnessed recently in community contributions to Google Sky, the value added for public interest and interaction is enormous. LSST will allow people to see that they are part of a dynamic Universe. User-friendly visualization interfaces will enable new research as well as being a vehicle for education and public involvement. Elementary school students in Earth science classes can participate in the discovery of new asteroids. High school and college students can discover supernovae and measure their light curves, thereby learning about both measurement processes and cosmology. The implications for all levels of scientific, engineering, and technical education cannot be overstated.

The LSST Education and Public Outreach (EPO) program will provide tools for the public, museum visitors, and students not only to examine and understand the achievements of LSST, but also to participate in the process of scientific discovery. With partners and collaborators such as the Google Corporation, the American Museum of Natural History, the Las Cumbres Observatory Global Telescope Network, and others, a number

of innovative programs have been devised: an internet-based public outreach system called involving citizen-scientists, advanced visualization demonstrations at the Hayden and Adler planetaria, formal educational programs focused on solar system science and cosmology, teacher training, and the development of new software EPO tools. LSST is perfectly positioned to bring such a transformative EPO program to fruition.

7. SUMMARY AND CONCLUSIONS

Until recently, most astronomical investigations have focused on small samples of cosmic sources or individual objects. Over the past decade, however, advances in technology have made it possible to move beyond the traditional observational paradigm and to undertake large-scale sky surveys, such as SDSS, 2MASS, GALEX and many others. This observational progress, based on a synergy of advances in telescope construction, detectors, and above all, information technology, has had a dramatic impact on nearly all fields of astronomy, many areas of fundamental physics, and society in general. The LSST builds on the experience of these surveys and addresses the broad goals stated in several nationally endorsed reports by the U.S. National Academy of Sciences.

The realization of the LSST involves extraordinary engineering and technological challenges: the fabrication of large, high-precision optics; construction of a huge, highly-integrated array of sensitive, wide-band imaging sensors; and the operation of a data management facility handling tens of terabytes of data each day. The design and development effort, which has been underway since 2006 and will continue through the onset of construction, includes structural, thermal, and optical analyses of all key hardware subsystems, vendor interactions to determine manufacturability, explicit prototyping of high-risk elements, prototyping and development of data management systems, and extensive systems engineering studies. Over 100 technical personnel at a range of institutions are currently engaged in this program.

In September 2007, LSST passed the NSF Conceptual Design Review for construction, which puts it on track for the Preliminary Design Review around the end of 2008. The casting of the primary/tertiary mirror is in progress⁵⁵ and it reached a peak temperature of approximately 1165 °C on March 29th, 2008. The LSST design and development phase will continue for another 3 years under NSF support along with in-kind contributions and private gifts. It is proposed that the U.S. Department of Energy support the cost of constructing the camera. LSST has high visibility in the high-energy physics community, both at universities and government laboratories. The project is scheduled to have first light in 2014 and the beginning of survey operations in 2015.

The LSST survey will open a movie-like window on objects that change brightness, or move, on timescales ranging from 10 seconds to 10 years. The survey will have a data rate of about 30 TB/night (more than one complete Sloan Digital Sky Survey per night), and will collect over 60 PB of raw data over its lifetime, resulting in an incredibly rich and extensive public archive that will be a treasure trove for breakthroughs in many areas of astronomy and physics. About 10 billion galaxies

⁵⁴ At the angular resolution of LSST, it would take over 3 million HDTV sets (with 1080×1920 pixel resolution) to display a single-epoch LSST image of half the Celestial Sphere (and about 1000 such images will be obtained over 10 years).

⁵⁵ Please see http://www.lsst.org/News/highfire_event.shtml

and a similar number of stars will be detected – *for the first time in history, the number of cataloged celestial objects will exceed the number of living people!* About a thousand observations of each position across half of the Celestial Sphere will represent the greatest movie of all time: assuming HDTV resolution (2.1 Mpix/frame) with 30 frames per second, and 270 color images per position (e.g., the *ugr* and *izy* color-composites, c.f. Table 1), it would take about eleven uninterrupted months to view this color movie (equivalent to about 4,000 feature films).

The cost estimate for LSST is \$389M for construction and \$37M per year for operations (in 2006 U.S. dollars). LSST will be much more efficient than the current state-of-the-art massive optical survey, the SDSS. For example, for each \$100 spent, the SDSS obtained single-epoch *ugriz* photometry for ~ 200 sources and a spectrum for a single source. In contrast, for \$100 LSST will obtain *ugrizy* photometry for more than 2,000 sources (to a limit 5 magnitudes deeper than SDSS) and a 1000-point light curve for ~ 200 sources. Compared to the SDSS, LSST will produce about 2,000 times larger data volume with an increase in total cost of less than a factor of ten.

LSST has been conceived as a public facility: the database that it will produce, and the associated object catalogs that are generated from that database, will be made available to the world’s scientific community and to the public at large with no proprietary period. The software which creates the LSST database will be open source. *LSST will be a significant milestone in the globalization of the information revolution.* LSST will put terabytes of data each night into the hands of anyone that wants to explore it, and in some sense will become an internet telescope: the ultimate network peripheral device to explore the Universe, and a shared resource for all humanity.

ACKNOWLEDGMENTS

In 2003, the LSST Corporation was formed as a non-profit 501(c)3 Arizona corporation with headquarters in Tucson, AZ. Membership has since expanded to more than twenty members including Brookhaven National

Laboratory, California Institute of Technology, Carnegie Mellon University, Columbia University, Google Inc., Harvard-Smithsonian Center for Astrophysics, Johns Hopkins University, Kavli Institute for Particle Astrophysics and Cosmology - Stanford University, Las Cumbres Observatory Global Telescope Network, Inc., Lawrence Livermore National Laboratory, National Optical Astronomy Observatory, Princeton University, Purdue University, Research Corporation, Stanford Linear Accelerator Center, The Pennsylvania State University, The University of Arizona, University of California at Davis, University of California at Irvine, University of Illinois at Urbana-Champaign, University of Pennsylvania, University of Pittsburgh, and the University of Washington. LSST is a public-private partnership. Design and development activity is supported by in part the National Science Foundation under Scientific Program Order No. 9 (AST-0551161), Scientific Program Order No. 1 (AST-0244680) through Cooperative Agreement AST-0132798, and grant AST-0441069. Portions of this work are supported by the Department of Energy under contract DE-AC02-76SF00515 with the Stanford Linear Accelerator Center, contract DE-AC02-98CH10886 with Brookhaven National Laboratory, contract DE-AC52-07NA27344 with Lawrence Livermore National Laboratory, and grant DE-FG02-07ER41505. A portion of this work was conducted at the Jet Propulsion Laboratory, California Institute of Technology, under a contract with NASA. Gifts by the Charles Simonyi Fund for Arts and Sciences, and Bill Gates, and grants by W. M. Keck Foundation and the TABASGO Foundation are gratefully acknowledged. Additional funding comes from private gifts, grants to universities, and in-kind support at Department of Energy laboratories and other LSSTC Institutional Members.

NOAO is operated by the Association of Universities for Research in Astronomy, Inc. (AURA) under cooperative agreement with the National Science Foundation.

We thank Chris Borden, Seth Digel, Tim Knauer and Branimir Sesar for valuable comments.

APPENDIX

Version History

Version 1.0: the first posting.

REFERENCES

- Adelman-McCarthy, J.K., Agüeros, M.A., Allam, S.S., et al. 2006, *Astrophysical Journal Supp.*, 162, 38
- A’Hearn, M.F. 2004, in *Comets II*, M.C. Festou, H.U. Keller, and H.A. Weaver (eds.), University of Arizona Press, Tucson, 745 pp., p.17-22
- Albrecht, A. & Bernstein, G. 2007, *Physical Review D*, 75, 3003
- Albrecht, A., Bernstein, G., Cahn, R., et al. 2006, *astro-ph/0609591*
- Alcock, C., Allsman, R.A., Alves, D.R., et al. 2000, *Astrophysical Journal*, 542, 281
- Anderson, G.P., Berk, A., Acharya, P.K., et al. 1999, in “Optics in Atmospheric Propagation and Adaptive Systems III”, A. Kohnle & J.D. Gonglewski, eds., *Proceedings of the SPIE*, 3866, 2
- Angel, R., Lesser, M. & Sarlot, R. 2000, in “Imaging the Universe in Three Dimensions: Astrophysics with Advanced Multi-wavelength Imaging Devices”, W. Bruegel and J. Bland-Hawthorn, eds., *ASP Conference Series*, 195, 81
- Barnard, M., Abrahamse, A., Albrecht, A., Bozek, B. & Yashar, M., *astro-ph/0804.0413*
- Bartelmann, M. & Schneider, P. 2001, *Physics Reports*, 340, 291
- Bartelmann, M., Huss, A., Colberg, J.M., Jenkins, A. & Pearce, F.R. 1998, *Astronomy & Astrophysics*, 330, 1
- Beaulieu, J.P., Bennett, D.P., Fouqué, P., et al. 2006, *Nature*, 439, 437
- Becker, A.C., Wittman, D.M., Boeshaar, P.C., et al. 2004, *Astrophysical Journal*, 611, 418
- Becker, R.H., White, R.L., & Helfand, D.J. 1995, *Astrophysical Journal*, 450, 559
- Bell, E.F., Zucker, D.B., Belokurov, V. et al. 2007, accepted to *Astrophysical Journal* (also *astro-ph/0706.0004*)
- Belokurov, V., Zucker, D.B., Evans, N.W., et al. 2007a, *Astrophysical Journal*, 654, 897
- Belokurov, V., Evans, N.W., Moiseev, A., et al. 2007b, *Astrophysical Journal*, 671, L9
- Bernstein, G.M., Trilling, D.E., Allen, R.L., et al. 2004, *Astronomical Journal*, 128, 1364
- Blake, C. & Glazebrook, K. 2003, *Astrophysical Journal*, 594, 665
- Blandford, R.D., Marshall, P., Oguri, M., et al. 2008, *American Astronomical Society, AAS Meeting #211, #137.07*
- Bloom, J.S., Perley, D.A., Li, W., et al. 2008, *astro-ph/0803.3215*

- Bottke, W.F., Vokrouhlický, D., Brož, M., Nesvorný, D. & Morbidelli, A. 2001, *Science*, 294, 1693
- Brandt, N., Anderson, S.F., Ballantyne, D.R., et al. 2007, *American Astronomical Society, AAS Meeting #211, #137.09*
- Briceno, C., Calvet, N., Hernandez, J., et al. 2005, *Astronomical Journal*, 129, 907
- Brown, M.E., Trujillo, C. & Rabinowitz, D. 2004, *Astrophysical Journal*, 617, 645
- Budavári, T., Connolly, A.J., Szalay, A.S., et al. 2003, *Astrophysical Journal*, 595, 59
- Bullock, J.S. & Johnston, K.V. 2005, *Astrophysical Journal*, 635, 931
- Burke, D., Axelrod, T., Bartlett, J., et al. 2007, *American Astronomical Society, AAS Meeting #211, #137.23*
- Carollo, D., Beers, T.C., Lee, Y.S., et al. 2007, *Nature*, 450, 1020
- Casetti-Dinescu, D.I., Girard, T.M., Herrera, D., et al. 2007, *Astronomical Journal*, 134, 195
- Charbonneau, D., Brown, T.M., Latham, D.W. & Mayor, M. 2000, *Astrophysical Journal*, 529, L45
- Clem, J.L., VandenBerg, D.A. & Stetson, P. 2008, *Astronomical Journal*, 135, 682
- Cole, S., Percival, W.J., Peacock, J.A., et al. 2005, *Monthly Notices of the Royal Astronomical Society*, 362, 505
- Cooray, A.R. 1999, *Astronomy & Astrophysics*, 348, 31
- Cooray, A.R., Hu, W., Huterer, D. & Joffe, M. 2001, *Astrophysical Journal*, 557, L7
- Cowan, N. & Ivezić, Ž. 2008, *Astrophysical Journal*, 674, L13
- Dandy, C.L., Fitzsimmons, A. & Collander-Brown, S.J. 2002, *Icarus*, 163, 363
- de Jong, J.T.A., Kuijken, K.H. & Héraudeau, P. 2008, *Astronomy & Astrophysics*, 478, 755
- de Vries, W.H., Becker, R.H., & White, R.L. 2003, *Astronomical Journal*, 126, 1217
- Dolney, D., Jain, B. & Takada, M. 2006, *MNRAS*, 366, 884
- Doressoundiram, A., Peixinho, N., Moullet, A., et al. 2007, *Astronomical Journal*, 134, 2186
- Duncan, M.J. & Levison, H.F. & Budd, S.M. 1995, *Astronomical Journal*, 110, 3073
- Eisenstein, D.J., Zehavi, I., Hogg, D.W., et al. 2005, *Astrophysical Journal*, 633, 560
- Eisenstein, D.J., Hu, W. & Tegmark, M. 1998, *Astrophysical Journal*, 504, L57
- Elliot, J.L., Kern, S.D., Clancy, K.B., et al. 2005, *Astronomical Journal*, 129, 1117
- Evans, C.R. & Kochanek, C.S. 1989, *Astrophysical Journal*, 346, L13
- Flaugher, B. 2006, *Proc. of SPIE*, Vol. 6269, 62692C
- Fukugita, M., Ichikawa, T., Gunn, J.E., et al. 1996, *Astronomical Journal*, 111, 1748
- Gardner, J.P., Mather, J.C., Clampin, M., et al. 2006, *Space Science Reviews*, 123, 485
- Garnavich, P.M., Smith, R.C., Miknaitis, G., et al. 2005, *American Astronomical Society, AAS Meeting #205, #108.18*
- Gee, P., Tyson, J.A., Pinto, P., et al. 2007, *American Astronomical Society, AAS Meeting #211, #137.28*
- Gezari, S., Basa, S., Martin, D.C., et al. 2008, *Astrophysical Journal*, 676, 944
- Girard, T.M., Korchagin, V.I., Casetti-Dinescu, D.I., et al. 2006, *Astronomical Journal*, 132, 1768
- Gladman, B., Kavelaars, J.J., Petit, J.-M., et al. 2001, *Astronomical Journal*, 122, 1051
- Gratton, R.G., Fusi Pecci, F., Carretta, E., et al. 1997, *Astrophysical Journal*, 491, 749
- Grillmair, C.J. 2006a, *Astrophysical Journal*, 645, L37
- Grillmair, C.J. 2006b, *Astrophysical Journal*, 651, L29
- Gunn, J.E., Carr, M., Rockosi, C., et al. 1998, *Astronomical Journal*, 116, 3040
- Gunn, J.E., Siegmund, W.A., Mannery, E.J., et al. 2006, *Astronomical Journal*, 131, 2332
- Hannestad, S., Tu, H. & Wong, Y.Y. 2006, *Journal of Cosmology and Astroparticle Physics*, 6, 25
- Helmi, A., Ivezić, Ž., Prada, F., et al. 2003, *Astrophysical Journal*, 586, 195
- Hoeflich, P., Wheeler, J.C. & Thielemann, F.K. 1998, *Astrophysical Journal*, 495, 617
- Howell, D.A., Sullivan, M., Conley, A. & Carlberg, R. 2007, *Astrophysical Journal*, 667, 37
- Hu, W. & Tegmark, M. 1999, *Astrophysical Journal*, 514, L65
- Hu, W. & Haiman, Z. 2003, *Physical Review D*, 68, 063004
- Hu, W. & Jain, B. 2004, *Physical Review D*, 70, 3009
- Huterer, D., Takada, M., Bernstein, G. & Jain, B. 2006, *MNRAS*, 366, 101
- Ibata, R., Irwin, M., Lewis, G.F. & Stolte, A. 2001, *Astrophysical Journal*, 547, L133
- Ibata, R., Martin, N.F., Irwin, M., et al. 2007, *Astrophysical Journal*, 671, 1591
- Ishak, M., Upadhye, A. & Spergel, D.N. 2006, *Physical Review D*, 74, 043513
- Ivezić, Ž., Tabachnik, S., Rafikov, R., et al. 2001, *Astronomical Journal*, 122, 2749
- Ivezić, Ž., Lupton, R.H., Schlegel, D., et al. 2003, *astro-ph/0309075*
- Ivezić, Ž., Tyson, J.A., Jurić, M. et al. 2007a, *Proceedings of IAU Symposium 236*. Edited by G.B. Valsecchi and D. Vokrouhlický. Cambridge: Cambridge University Press, 353 (also *astro-ph/0701506*)
- Ivezić, Ž., Smith, J. A., Miknaitis, G., et al. 2007b, *Astronomical Journal*, 134, 973
- Ivezić, Ž. 2007c, *ASP Conference Series*, Vol. 378, 485 (also *astro-ph/0701507*)
- Ivezić, Ž., Sesar, B., Jurić, M., et al. 2008, accepted to *Astrophysical Journal* (also *astro-ph/0804.3850*)
- Jain, B. & Taylor, A. 2003, *Physical Review Letters*, 91, 1302
- Jain, B. & Zhang, P. 2007, *astro-ph/0709.2375*
- Jedicke, R., Nesvorný, D., Whiteley, R., Ivezić, Ž., & Jurić, M. 2004, *Nature*, 429, 275
- Jedicke, R., Denneau, L., Grav, T., et al. 2005, *American Astronomical Society, AAS Meeting #207, #121.02*
- Jewitt, D.C., Trujillo, C.A. & Luu, J.X. 2000, *Astronomical Journal*, 120, 1140
- Jones, R.L., Gladman, B., Petit, J.-M., et al. 2006, *Icarus*, 185, 508
- Jones, R.L., Chesley, S., Connolly, A.J., et al. 2007, *American Astronomical Society, AAS Meeting #211, #137.14*
- Jurić, M., Ivezić, Ž., Brooks, A., et al. 2008, *Astrophysical Journal*, 673, 864
- Kaiser, N., Aussel, H., Burke, B.E., et al. 2002, in “Survey and Other Telescope Technologies and Discoveries”, Tyson, J.A. & Wolff, S., eds. *Proceedings of the SPIE*, 4836, 154
- Kalirai, J.S., Hansen, B.M.S., Kelson, D.D., et al. 2008, *Astrophysical Journal*, 676, 594
- Kalirai, J.S., Richer, H.B., Fahlman, G.G., et al. 2001, *Astronomical Journal*, 122, 257
- Kan, F.W. & Antebi, J. 2003, in “Future Giant Telescopes”, Angel, J.R.P. & Gilmozzi, R., eds., *Proceedings of the SPIE*, 4840, 485
- Kashikawa, N., Takata, T., Ohya, Y., et al. 2003, *Astronomical Journal*, 125, 53
- Kaspi, S., Brandt, W.N., Maoz, D., et al. 2007, *Astrophysical Journal*, 659, 997
- Keller, S.C., Schmidt, B.P., Bessell, M.S., et al. 2007, *Publications of the Astronomical Society of Australia*, 24, 1
- Knežević, Z. & Milani, A. 2005, *Highlights of Astronomy*, Ed. O. Engvold. San Francisco, CA, p. 758
- Knox, L., Song, Y., Tyson, J.A. 2006, *Physical Review D*, 74, 3512
- Konacki, M., Torres, G., Jha, S. & Sasselov, D.D. 2003, *Nature*, 421, 507
- Kulkarni, S. 2006, Presented at the KITP Conference: Transient Universe: Popular, Not so Popular & Knowable Unknowns, Mar 13, 2006, Kavli Institute for Theoretical Physics, University of California, Santa Barbara
- Kundić, T., Turner, E.L., Colley, W.N., et al. 1997, *Astrophysical Journal*, 482, 75
- Kurucz, R.L. 1979, *Astrophysical Journal Supp.*, 40, 1
- Law, D.R., Johnston, K.V. & Majewski, S.R. 2005, *Astrophysical Journal*, 619, 807
- Lenz, D.D., Newberg, J., Rosner, R., et al. 1998, *Astrophysical Journal Supp.*, 119, 121
- Lepine, S. 2008, *astro-ph/0803.4203*
- Lepine, S. & Scholz, R.-D. 2008, *astro-ph/0804.1731*
- Linder, E.V. 2003, *Physical Review D*, 68, 083504
- Liu, H.T., Bai, J.M., Zhao, X.H. & Ma, L. 2008, *Astrophysical Journal*, 677, 884
- Lowry, S.C., Fitzsimmons, A., Cartwright, I.M. & Williams, I.P. 1999, *Astronomy & Astrophysics*, 349, 649
- Lucas, P.W. & Roche, P.F. 2000, *MNRAS*, 314, 858
- Lue, A., Scoccimarro, R. & Starkman, G. 2004, *Physical Review D*, 69, 4005

- Majewski, S.R., Skrutskie, M.F., Weinberg, M.D. & Ostheimer, J.C. 2003, *Astrophysical Journal*, 599, 1082
- Mandelbaum, R., Seljak, U., Kauffmann, G., Hirata, C.M. & Brinkmann, J. 2006, *MNRAS*, 368, 715
- Martin, D.C., Fanson, J., Schiminovich, D., et al. 2006, *Astrophysical Journal*, 619, L1
- Martini, P. & Schneider, D.P. 2003, *Astrophysical Journal*, 597, 109
- Mathieu, R. 2000, *Proceedings from ASP Conference*, 198, R. Pallavicini, G. Micela, and S. Sciortino, eds. 517
- McGehee, P.M. 2004, *Proceedings of ASP Conference* 317. D. Clemens, R.Shah, and T. Brainerd, eds. San Francisco: Astronomical Society of the Pacific, p.199
- Meyer, J.M., Ivezić, Ž., Finkbeiner, D.P., et al. 2005, *American Astronomical Society, AAS Meeting #207*, #131.01
- Monet, D.G., Levine, S.E., Canzian, B., et al. 2003, *Astronomical Journal*, 125, 984
- Morokuma, T., Inada, N., Oguri, M., et al. 2007, *Astronomical Journal*, 133, 214
- Morokuma, T., Mamoru D., Naoki Y., et al. 2008, *Astrophysical Journal*, 676, 163
- Munn, J.A., Monet, D.G., Levine, S.E., et al. 2004, *Astronomical Journal*, 127, 3034
- Neill, J.D. & Shara, M.M. 2005, *Astronomical Journal*, 129, 1873
- Nemiroff, R.J. 2003, *Astronomical Journal*, 125, 2740
- Nesvorný, D., Jedicke, R., Whiteley, R. & Ivezić, Ž. 2005, *Icarus* 173, 132
- Newman, J., 2008, *astro-ph/0805.1409*
- Oguri, M. & Kawano, Y. 2003, *MNRAS*, 338, L25
- Padmanabhan, N., Schlegel, D., Finkbeiner, D., et al. 2008, *Astrophysical Journal*, 674, 1217
- Parker, A., Ivezić, Ž., Jurić, M., et al. 2008, submitted to *Icarus*
- Perlmutter, S., Aldering, G., Goldhaber, G., et al. 1999, *Astrophysical Journal*, 517, 565
- Perryman, M.A.C., de Boer, K.S., Gilmore, G., et al. 2001; *Astronomy & Astrophysics*, 369, 339
- Pier, J.R., Munn, J.A., Hindsley, R.B., et al. 2003, *Astronomical Journal*, 125, 1559
- Pinto, P.A., Smith, R.C., Garnavich, P.M., et al. 2005, *American Astronomical Society, AAS Meeting #205*, #108.20
- Porciani, C. & Madau, P. 2000, *Astrophysical Journal*, 532, 679
- Pravec, P. & Harris, A.W. 2000, *Icarus*, 148, 12
- Rabinowitz, D.L. 1993, *Astrophysical Journal*, 407, 412
- Richards, G.T., Fan, X., Newberg, H.J., et al. 2002, *Astronomical Journal*, 123, 2945
- Riess, A.G., Filippenko, A.V., Challis, P., et al. 1998, *Astronomical Journal*, 116, 1009
- Riess, A.G., Strolger, L-G., Casertano, S., et al. 2007, *Astrophysical Journal*, 659, 98
- Saha, A., Olsen, K., Monet, D.G., et al. 2007, *American Astronomical Society, AAS Meeting #211*, #137.13
- Scranton, R., Connolly, A., Krughoff, S., et al. 2007, *astro-ph/0709.0752*
- Seljak, U., Makarov, A., McDonald, P., et al. 2005, *Physical Review D*, 71, 3515
- Seo, H.-J. & Eisenstein, D.J. 2003, *Astrophysical Journal*, 598, 720
- Sesar, B., Ivezić, Ž., Lupton, R.H., et al. 2007, *Astronomical Journal*, 134, 2236
- Shields, G.A. & Bonning, E.W. 2008, *astro-ph/0802.3873*
- Skrutskie, M.F., Cutri, R.M., Stiening, R., et al. 2006, *Astronomical Journal*, 131, 1163.
- Smolčić, V., Ivezić, Ž., Knapp, G.R., et al. 2004, *Astrophysical Journal*, 615, L141
- Song, Y.-S. & Knox, L. 2004, *Physical Review D*, 70, 63510
- Spergel, D.N., Verde, L., Peiris, H.V., et al. 2007, *Astrophysical Journal Supp.*, 148, 175
- Strauss, M.A. 2007, *American Astronomical Society, AAS Meeting #211*, #137.04
- Stubbs, C.W. & Tonry, J., 2006, *Astrophysical Journal*, 646, 1436
- Stubbs, C.W., High, F.W., George, M.R., et al. 2007, *PASP*, 119, 1163
- Szabó, Gy.M., Ivezić, Ž., Jurić, M., & Lupton, R. 2007, *MNRAS*, 377, 1393
- Takada, M. & Jain, B. 2004, *MNRAS*, 348, 897
- Tegmark, M., Eisenstein, D.J., Strauss, M.A., et al. 2006, *Physical Review D*, 74, 3507
- Tokovinin, A. 2002, *PASP*, 114, 1156
- Trujillo, C.A., Jewitt, D.C. & Luu, J.X. 2001, *Astronomical Journal*, 122, 457
- Tyson, J.A., Kochanski, G.P. & Dell’Antonio, I.P. 1998, *Astrophysical Journal*, 498, L107
- Tyson, J.A. 2006, *Nature*, 442, 364
- Tyson, J.A., Roat, C., Bosch, J. & Wittman, D. 2008, *Astronomical Data Analysis Software and Systems XVII*, ASP Conference Series, J. Lewis, R. Argyle, P. Bunclark, D. Evans, and E. Gonzales-Solares, eds.
- Vanden Berk, D.E., Wilhite, B.C., Kron, R.G., et al. 2004, *Astrophysical Journal*, 601, 692
- Walsh, S.M., Jerjen, H. & Willman, B. 2007, *Astrophysical Journal*, 662, L83
- Wang, S., Haiman, Z., May, M. & Kehayias, J. 2005, *astro-ph/0512513*
- West, A.A., Hawley, S.L., Walkowicz, L.M., et al. 2004, *Astronomical Journal*, 128, 426
- Wittman, D.M., Tyson, J.A., Kirkman, D., Dell’Antonio, I. & Bernstein, G. 2000, *Nature*, 405, 143
- Wood-Vasey, W.M., Miknaitis, G., Stubbs, C.W., et al. 2007, *Astrophysical Journal*, 666, 694
- Yoo, J., Chanamé, J. & Gould, A. 2004, *Astrophysical Journal*, 601, 311
- York, D.G., Adelman, J., Anderson, S., et al. 2000, *Astronomical Journal*, 120, 1579
- Yoshida, F. & Nakamura, T. 2005, *Astronomical Journal*, 130, 2900
- Zhan, H. 2006, *Journal of Cosmology & Astroparticle Physics*, 8, 8
- Zhan, H. & Knox, L. 2006, *Astrophysical Journal*, 644, 663
- Zhang, B. & Mészáros, P. 2004, *International Journal of Modern Physics A*, 19, 2385